

Chapter 5

IN SITU TOTAL ELECTRON-YIELD XAFS INVESTIGATIONS OF A CU/ZNO/AL₂O₃ METHANOL SYNTHESIS CATALYST

5.1. Introduction

Introduced by ICI in the mid-1960s, promoted Cu/ZnO formulations are still the most widely used methanol synthesis catalysts found in industrial practice [1,2]. The synthesis is typically operated at 50-100 bar and 493-523 K, using a feed containing CO, CO₂, and H₂ ("syngas") [2]. A considerable amount of work has been devoted to the study of the surface chemistry underlying the process, at least in part driven by expectations of large future market for fuels which are based on or derived from methanol (see, e.g. ref. [3]). Space constraints simply do not allow here to discuss the immense body of literature on the subject in detail (a list of reviews and articles with background information includes refs. [1,2,4-14]). Both the chemical state of the catalyst and details of the reaction mechanism are still the issues of lively debates (see, e.g., refs. [15-37]). It is quite well established that the reaction sequence involves the catalytic hydrogenation of CO₂ to the methanol molecule or a precursor of it, since kinetic and isotope labelling experiments prove that CO₂ is the source of the carbon in the final product (see refs. [2,13,15,32,38-42]). The reaction sequence is believed to proceed on the surface of the Cu particles. Evidence for this view comes from a variety of experiments (see, e.g., refs. [2,12,18,38,43-47]), most notably single crystal studies, which have shown that atomically flat Cu surfaces synthesise methanol [48-50] with a reaction rate comparable to that of the industrial catalyst [50,51]. The mechanistic details of CO₂-activation on Cu are still not fully understood. It has been suggested that the reaction requires a submonolayer of adsorbed oxygen atoms on the surface of Cu which act both as promoters and reactants in the course of the synthesis. Most of the evidence for partially oxidised Cu surfaces is based on post-reaction surface area titrations by reactive frontal chromatography with N₂O [29,43,52-55]. The reliability of results acquired by this method has been criticised, however, for reasons of non-invasiveness and the possibility of side-reactions with H₂ present in/on the oxidic catalyst supports [31,56-59]. It has been proposed that sintering of the Cu particles provides an alternative explanation for the results of N₂O titration [15,30], while transient CO titrations have shown that oxygen species in/on the *working* catalyst, if present at all, do not react

with CO under a syngas pressure of 1 atm [15,60]. In line with this, a previously published *in situ* study of the system by post-reaction TEY XAFS claimed that treatment of the catalyst with synthesis gas (1% CO, 1% CO₂, 8% H₂, 90% He) at 1 atm and 523 K for 30 min did not lead to detectable changes of the Cu K-edge XAFS [61]. Several other XAFS studies by transmission and fluorescence-yield (FY) detection have also drawn the conclusion [37,62-68] that the principal Cu component of the catalyst is in the zerovalent, metallic state.

Somewhat surprisingly, however, the results of the previous TEY XAFS study suggested that the Cu component was significantly oxidised when the catalyst was treated with *pure* CO₂ (10% CO₂ / 90% He) at 523 K [61]. This result was difficult to explain, since it is well known that dissociation of CO₂ on clean Cu must overcome a large activation barrier (67 kJ/mol on Cu(110) [60] and 93 kJ/mol on Cu(100) [69,70]) so that CO₂ dissociation probabilities on clean, ordered Cu surfaces at 500 K should be between 10⁻⁸ and 10⁻¹¹ - too low to be consistent with the XAFS result. Further TEY XAFS measurements will therefore be reported here which have reinvestigated the interaction of CO₂ with the Cu/ZnO/Al₂O₃ catalyst.

Ongoing discussions in the literature are also concerned with the morphology and chemical state of the Cu particles in the active catalyst [32,37,63,65,71,72]. For example, it has been noted in several XAFS studies that the amplitudes of the Cu K-edge fine-structure were strongly reduced relative to the bulk Cu metal spectrum [37,61,64,73,74]. These observations, which are not due to 'thickness' and 'self-absorption' artefacts (cf. chapter 4), suggest the presence of very small Cu particles. In a recent XAFS study, it was further proposed that dynamic changes occur in the metallic Cu phase of the active Cu/ZnO/Al₂O₃ catalyst, with particle shapes and dispersion varying as a function of adsorbate coverage and temperature [32,37]. Most notable has been the suggestion that the particles might be wetting the surfaces of the ZnO crystallites under certain reaction conditions, resulting in flat, island-like Cu particles [37].

Most of the work described in this chapter deals with the behaviour of the Cu phase in the catalyst under so-called industrial pre-reduction [2,8] conditions. The *in situ* TEY XAFS studies addressed the following issues.

(i) *Catalyst Genesis* - The chemical state of Cu in the calcined precursor, in the reduced, activated catalyst and as a function of reduction conditions was investigated.

(ii) *State of Active Catalyst under Synthesis Conditions* - *In situ* experiments at elevated temperatures and pressures have been performed.

(iii) *Interaction of the Activated Catalyst with CO₂* - A previous *in situ* experiment on the CO₂-interaction with the catalyst [61] has been repeated.

5.2. Experimental

5.2.1. Apparatus and Chemicals

XAFS experiments were carried out in the *in situ* TEY cell described in section 2.6. Synchrotron light from beamline 8.1 of the EPSRC Daresbury Laboratory was used, with the storage ring operating at 2 GeV. Ring currents varied between 140 mA and 240 mA. Rejection of beam harmonics was performed by detuning the double crystal Si(220) monochromator to 50% of reflectivity. Focusing of the beam was achieved by a Pt-coated toroidal mirror. The resulting X-ray flux was monitored by an ion chamber (20% absorption) filled with an Ar/He mixture.

The calcined (300°C) catalyst (supplied by ICI Katalco) containing 60 wt% CuO, 30 wt% ZnO and 10 wt% Al₂O₃ has previously been extensively characterised by a variety of techniques [8,12,53,75]. For XAFS measurements, samples were ground in a mortar, slurried onto the sample plate as a dispersion in iso-propanol, and dried at room temperature. Gases used in the experiments included He (Distillers MG 99.99%), blended air (99.9% pure, 80% N₂ / 20% O₂ mixture) and gas mixtures supplied by ECM Special Gases (5% H₂ in He, 10% CO₂ in He, impurity levels below 0.01%). Gas flows were controlled with a high-vacuum leak-tested gas-handling system based on stainless steel tubing (outer diameter: 1/4") with Swagelok[®] fittings and Nupro[®] bellows valves. Flow rates were measured with a commercial mass flow controller.

In situ XRD data were collected with an all-silica environmental cell [76] mounted on a Siemens D500 diffractometer. Data were acquired in reflection geometry, using Cu K_α radiation, in steps of $2\Theta = 0.02^\circ$ with a position-sensitive detector (PSD) subtending a solid angle of 6° . The resolution was enhanced with two narrow exit slits (width: $2\Theta = 0.15^\circ$) at the source, while the signal-to-background ratio was increased with a 10 mm Ni foil filter in front of the detector. Particle sizes were analysed using of the well-known Scherrer equation [77-79]

$$D = \frac{0.9 \cdot I}{\Delta(2\Theta) \cdot \cos\Theta} \quad (5.1)$$

where λ is the wavelength of the incident X-rays, Θ the X-ray incidence angle with respect to the sample surface and $\Delta(2\Theta)$ the broadening of the FWHM (in radians) in units of 2Θ relative to the instrumental resolution. A single peak variant [79] of the full line-shape analysis introduced by Warren and Auerbach [80] was also applied to the analysis of Cu metal particle sizes. The linewidth broadening $\Delta(2\Theta)$ for the Scherrer evaluations were obtained from pseudo-Voigt functions [79] fitted to the data, while Split Pearson VII functions were used for the full line-shape analysis [78,79].

5.2.2. Standard Samples

Standard XAFS spectra of Cu metal (Johnson Matthey, 99.99%, *in situ* reduced in 100% at 400°C), CuO (99.9% pure, Johnson Matthey Chemicals, U.K.) and Cu₂O (94% pure, containing approximately 6% CuO, BDH Ltd., U.K.) were recorded in TEY mode. All these data are presented with corresponding transmission data in Appendix B. The results of the EXAFS fitting analyses will also be reported below in tables 5.1 and 5.2 together with the catalyst results. Generally, no difficulties were encountered in analysing the crystallographic information in the standard data with EXCURV92. An exception was the derivation of the coordination information from the 2nd to 5th shell in CuO. These four shells are located at distances of 2.78 Å, 2.91 Å, 3.08 Å and 3.18 Å in the CuO lattice. Due to their close spacing, it is impossible to analyse them separately using Fourier filtering to isolate single shell contributions. This is illustrated by the imaginary part of the Fourier transformed EXAFS spectrum (fig. 5.1), which reveals that the minimum at $R \approx 3$ Å in the modulus of the Fourier transform is due to a ‘beat node’ between the contributions from the overlapping shells. The fitting results (listed below in table 5.1) therefore had to be obtained by careful simultaneous fitting of all shell parameters. Reproducible and physically meaningful best fits to the experimental EXAFS were only achieved (i) when the initial parameters for the refinement had been guessed quite accurately and (ii) when the 4th and 5th shell at 3.08 Å and 3.18 Å were modeled as a single shell. The quality of thus obtained best fits to the CuO spectrum can be judged from figure 5.1.

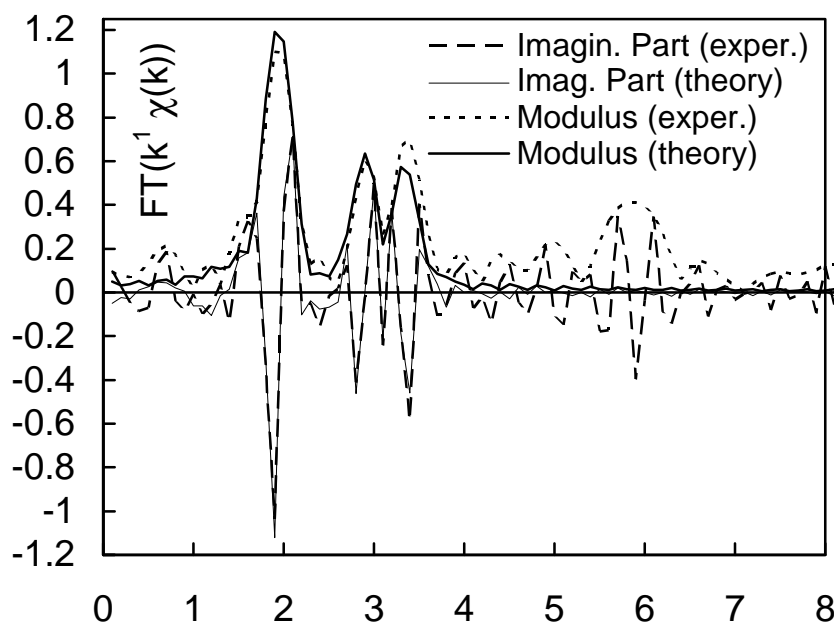


Figure 5.1. Fourier transforms (k -window: $3 \text{ \AA}^{-1} - 14 \text{ \AA}^{-1}$) of the experimental CuO data and the EXAFS fits including the first 5 coordination shells. The distance scale has not been corrected for the phaseshifts of the photoelectron wave at the central atom and the backscattering atom.

To allow an assessment of the influence of the promoter species (ZnO, Al₂O₃) on the XAFS results for the Cu component in the catalyst, a highly dispersed CuO precursor was also investigated. Using a stoichiometric amount of a 1.5 molar NaOH solution, this material was slowly (over the period of 1 h) precipitated from a vigorously stirred Cu(NO₃)₂ solution (1.5 molar in Cu²⁺, 50 ml) at 60°C. The resulting black slurry was aged in the reaction mixture at 60°C for 1 h, filtered, and then washed five times with ultra-pure, deionised (resistance: > 18 MΩ) water. The washed product was subsequently stored in glass vials at room temperature. Throughout the remainder of this chapter, this hydroxide-derived precursor will be referred to as “Cu(OH)₂”. Use of this label is, of course, not meant to imply that the composition of the material corresponds to stoichiometric Cu(OH)₂. It is textbook knowledge that Cu(OH)₂ tends to dehydrate to CuO under the present precipitation conditions. This is verified by an X-ray diffraction pattern of the wet precipitate (figure 5.2) which is dominated by the lines of CuO. Cu(OH)₂ is the minor component of the material (approximately 10%-20%). A line-broadening analysis using the Scherrer equation indicates that the particle size of the CuO crystallites is $120 \text{ \AA} \pm 30 \text{ \AA}$.

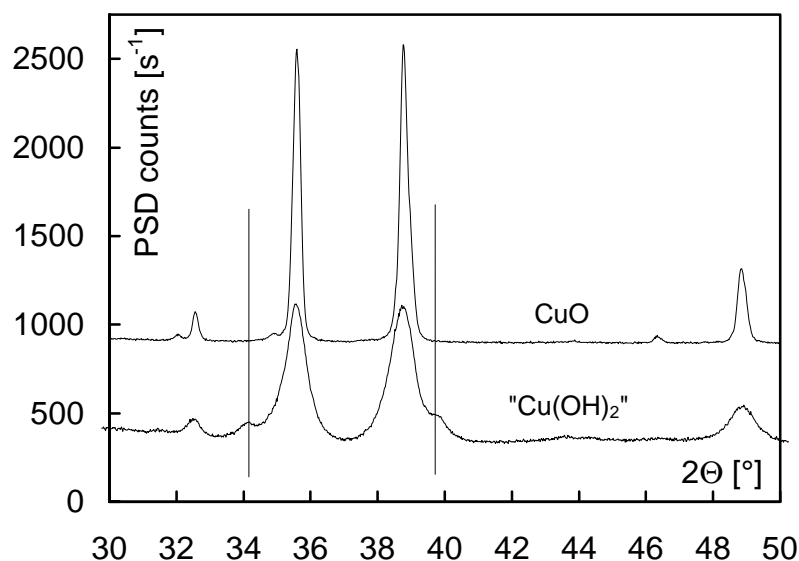


Figure 5.2. Comparison between parts of the diffraction patterns of basic CuO (freshly precipitated with NaOH) and the crystalline CuO standard. The broken lines indicate the positions of the additional lines due to residual Cu(OH)₂.

5.3. Results and Discussion

5.3.1. Calcined Catalyst Precursor

In line with previous XAFS studies of similar precursors [65,68,81-85], the Cu K-edge XANES (fig. 5.3) of the calcined catalyst is characteristic of CuO. Small differences to the near-edge spectrum of the crystalline CuO standard are nevertheless evident and can be summarised as a slight broadening of all spectral features. Such broadening is expected for highly dispersed and/or disordered materials. That it is the reason underlying the slight deviations between the XANES spectra is supported by a line broadening analysis (LBA) of the XRD pattern of the calcined sample. For the analysis, the diffractogram of the reduced sample was recorded and the difference pattern calculated (fig. 5.4). This approach allows to distinguish the CuO lines which are overlapping with the lines of the ZnO component in the diffraction pattern of the calcined sample. The CuO LBA has to be based on the Scherrer method because a full lineshape analysis could not be performed due to difficulties in modelling the pattern satisfactorily against the background of overlapping ZnO lines. The CuO particle size in the calcined material was thus estimated to be $70 \text{ \AA} \pm 30 \text{ \AA}$ ($\Delta(2\Theta) = 1.3$ at $2\Theta = 38.8^\circ$). Such particle sizes are of the order of magnitude for which changes in the XAFS due to surface effects should be noticeable (*vide infra*). Note, however, that the evaluation of the CuO lines in the difference pattern is not completely unambiguous, because it rests on the implicit assumption that changes to the pattern of the ZnO component can be neglected. That

some caution is necessary is indicated by XAFS data of the Zn K-edge. These data show that the order in the ZnO lattice increases during reduction, as borne out by the sharpening of all XANES features as well as an overall EXAFS amplitude increase (fig. 5.5).

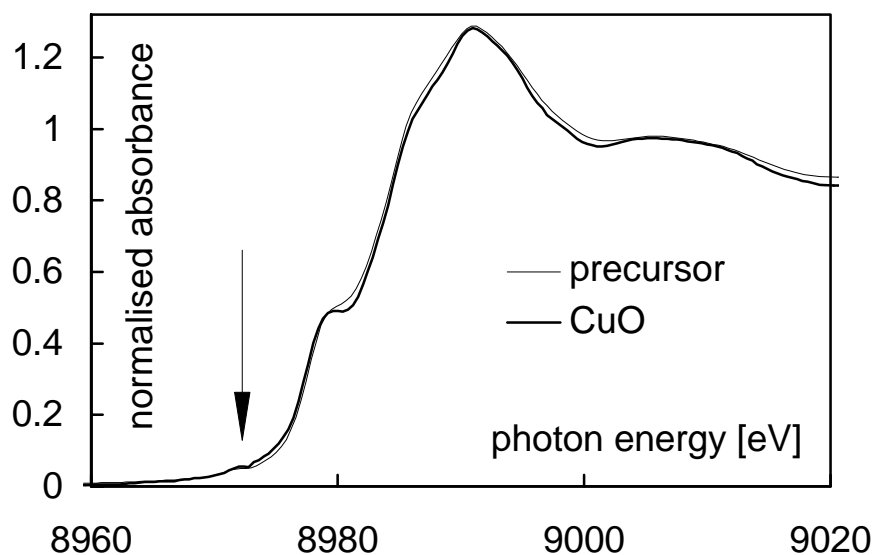


Figure 5.3. Near-edge spectrum of the calcined catalyst precursor (thin line) and crystalline CuO (thick line). The arrow indicates the position of the quadrupole-allowed Cu $1s \rightarrow 3d$ transition mentioned in the text.

The nevertheless quite good agreement between the Cu K-edge XANES spectra of the catalyst and CuO provides evidence that mixed oxide phases containing Zn²⁺ and Cu²⁺ are absent or present only in small concentrations. Note in this context that the intensity and shape of the weak pre-edge feature marked in figure 5.3 is identically present in both the catalyst and the CuO spectra. This pre-edge feature is due to quadrupole-allowed $1s \rightarrow 3d$ transitions in the Cu²⁺ ion [86] and is expected to become better resolved when the geometry of the first oxygen shell is tetrahedrally distorted from the tetragonal coordination in the CuO lattice [65,87]. Doping of Cu²⁺ into the tetrahedral sites of the ZnO lattice would therefore result in an enhancement of this transition - which is clearly not the case in the presented spectrum. An enhancement of this feature has, however, been observed in previous XAFS studies of Cu/ZnO catalysts with small Cu contents (1 wt% - 10 wt%) [65,87]. The incorporation of Cu in ZnO during calcination of Zn-rich precursors has also been inferred from XRD measurements and analytical electron microscopy investigations (cf. refs. [9,65,85,88-90]). It shall therefore not be excluded that Cu²⁺ concentrations below the XAFS detection limit (approximately 5%) might be doped into the ZnO lattice of the catalyst precursor.

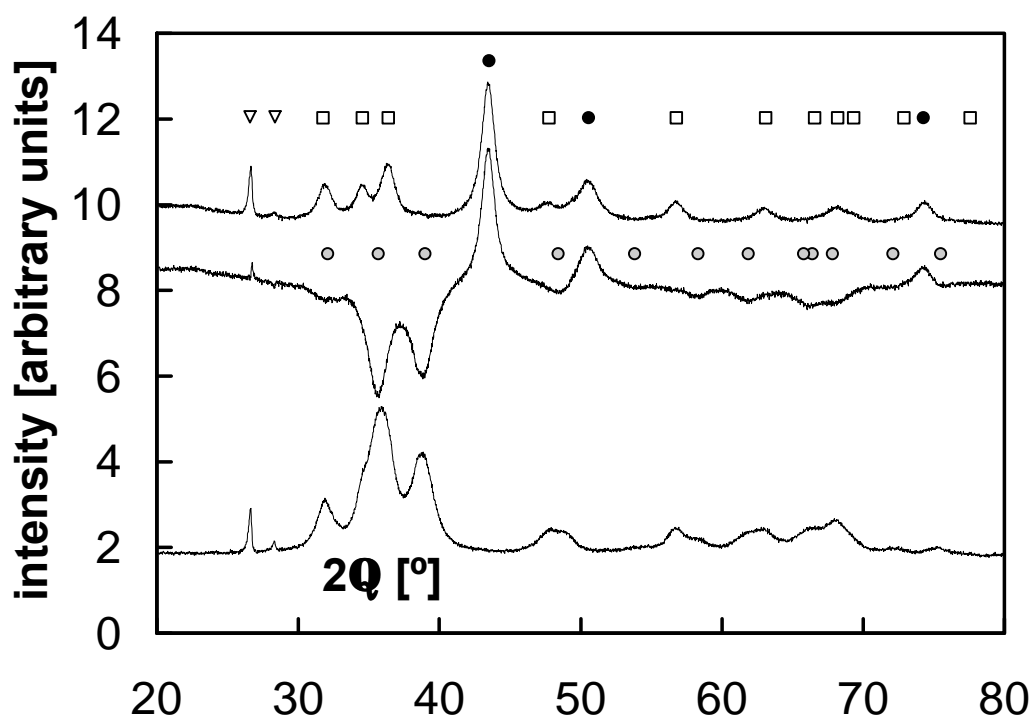


Figure 5.4. X-ray diffraction patterns of the calcined catalyst (bottom), the reduced catalyst (top), and their difference. Line assignments: Cu (black filled circles), CuO (grey filled circles), ZnO (open squares). The inverted triangles mark spurious reflection intrinsic to the experimental *in situ* setup.

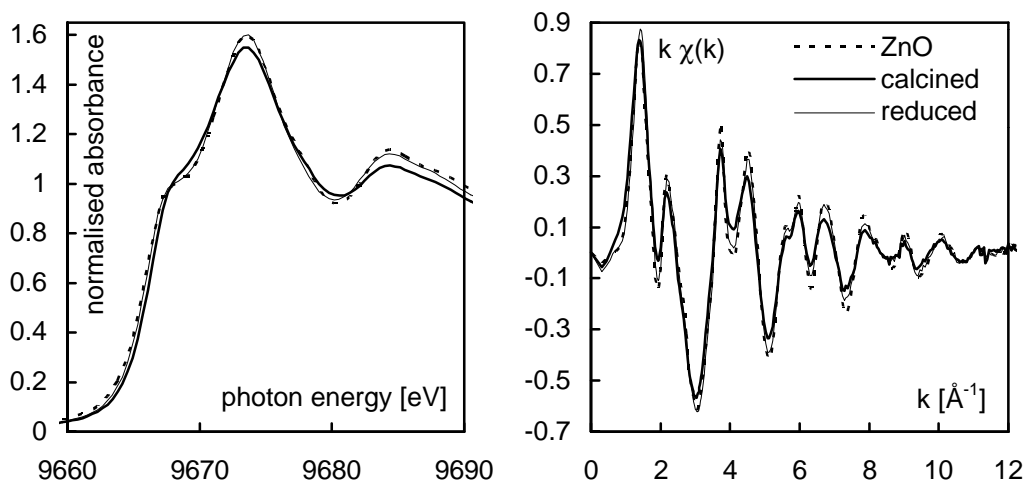


Figure 5.5. Near-edge and extended XAFS regions of the Zn K-edge spectra for the calcined catalyst precursor (thick full line), the reduced catalyst (thin full line) and a crystalline ZnO standard (thick broken line).

More detailed information on the precursor structure emerges from the examination of the Cu K-edge extended fine-structure. Figures 5.6 and 5.7 compare the EXAFS data and the corresponding Fourier transforms of the calcined catalyst to those of the “Cu(OH)₂” precursor and the CuO standard. It is seen that both the calcined catalyst and the hydroxide-derived precursor exhibit lowered EXAFS amplitudes relative to

CuO. The differences between the spectra are most pronounced in the k -range between 7 \AA^{-1} and 9 \AA^{-1} where strong high frequency oscillations due to long scattering paths are prominent in the CuO EXAFS. The strong damping of these scattering contributions in the EXAFS is a reliable indication for poor lattice order. This conclusion is supported by the fitting analysis (results given in table 5.1) as well as by the Fourier-transformed EXAFS spectra (fig. 5.7). The fitting analysis of the catalyst EXAFS yields Debye Waller factors which are larger than in CuO, except for the first coordination shell for which all amplitude parameters are, within the error margins, identical to those of crystalline CuO. This trend is also evident in the Fourier transforms, which show that damping of the information from more distant shells is comparatively stronger (fig. 5.7). All these results indicate that the first shell coordination of the Cu^{2+} ions in the catalyst has the square planar symmetry typical for the Cu^{2+} ion, while the coordination with more distant shells is characterised by increasing disorder. Note that the distances to all neighbouring shells appear also somewhat contracted (e.g., 1.950 \AA vs. 1.964 \AA for the first coordination shell, table 5.1). As will be discussed in a section below, this behaviour is expected for highly dispersed samples with large XAFS contributions from surface atoms [91].

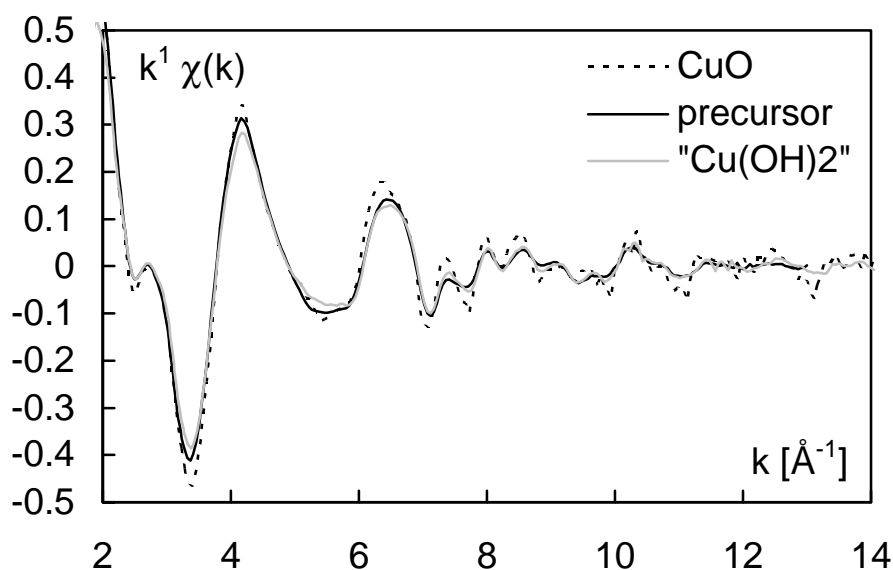
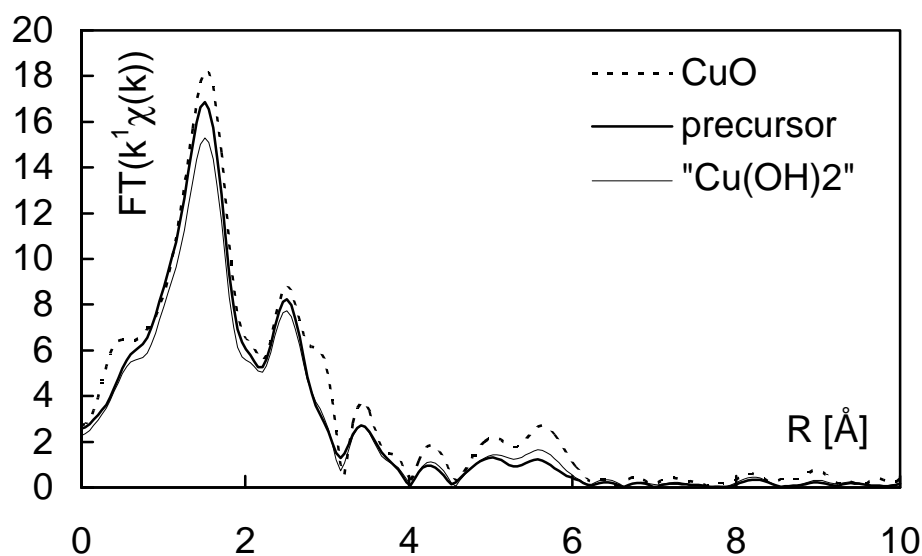


Figure 5.6. k^1 -weighted EXAFS data for the calcined catalyst precursor (black line), crystalline CuO (broken line) and the “Cu(OH)₂” reference precursor (grey line).

In summary, the combination of *in situ* X-ray diffraction and XAFS indicates that the Cu is essentially present as CuO, but disorder is noticeable even on a length scale of about 3 \AA . The result of the LBA suggests that a particle size effect on the XAFS due to the presence of a large amount of surface atoms is likely.

Table 5.1. Single-scattering fitting results for the calcined catalyst, “Cu(OH)₂”, Cu₂O and CuO.

	CuO standard	Cu ₂ O standard	“Cu(OH) ₂ ”	calcined catalyst
S_0^2	0.64 (2)	0.82 (2)	0.55 (2)	0.62 (2)
E_f [eV]	-10.7 (4)	-8.1 (3)	-9.5 (4)	-9.0 (5)
$N_1 \dots N_4$	4 / 2 / 4 / 6	2 / 12 / 6 / 6	4 / 2 / 4 / 6	4 / 2 / 4 / 6
R_1 [Å]	1.964 (4)	1.836 (4)	1.947 (4)	1.950 (4)
R_2 [Å]	2.78 (3)	3.007 (4)	2.72 (3)	2.70 (3)
R_3 [Å]	2.935 (7)	3.45 (2)	2.902 (7)	2.906 (7)
R_4 [Å]	3.122 (7)	4.26 (1)	3.083 (8)	3.083 (9)
s_1^2	0.004 (1)	0.009 (1)	0.005 (1)	0.006 (1)
s_2^2	0.012 (9)	0.046 (1)	0.017 (9)	0.03 (1)
s_3^2	0.008 (2)	0.055 (8)	0.010 (2)	0.013 (2)
s_4^2	0.012 (1)	0.034 (3)	0.018 (2)	0.024 (3)
k -range [Å ⁻¹]	3 - 14	3 - 12	3 - 13	3 - 13
R -factor	23.2	18.3	18.9	17.1

**Figure 5.7.** Moduli of the Fourier transforms of the spectra presented in fig. 5.6. Note for the spectra of the precursor and the “Cu(OH)₂” reference that the amplitude information from the coordination shells located below 3 Å is less damped than in the more distant shells. The distance scale has not been corrected for the phaseshifts of the photoelectron wave at the central atom and the backscattering atom.

5.3.2. Structure of the Reduced Catalyst

Before presenting XAFS results for the reduced catalyst it shall be pointed out that the reduction behaviour of the Cu component of the catalyst is very complex. Quite subtle changes in the XAFS spectra will show that the state of Cu in the reduced

catalyst is dependent on the final reduction temperature, the temperature gradient during reduction, the duration of reduction at the final temperature and also the partial pressure of H₂ in the reducing gas mixture. The importance of these preparation parameters is well known from industrial practice [2,8], but nevertheless not very well understood. Better knowledge of the reduction behaviour of the catalyst could provide key insights into the surface chemistry underlying methanol synthesis. XAFS evidence for catalyst morphology changes as a result of different reduction conditions have so far, at least to the authors knowledge, not been reported.

The spectra will be referenced against a TEY dataset obtained for a coarsely grained (particle sizes larger than 1 μm), powdered sample of metallic Cu (cf. section 5.2.2). Comparison of the catalyst data to a TEY standard ensures that systematic amplitude errors due to small 'self-absorbed' fluorescence and the possible effects of low X-ray incidence angles (cf. chapter 4) are eliminated from the analysis.

5.3.2.1. Extended Fine-Structure

A selection of representative EXCURV92 analysis results are given in table 5.2. All EXAFS data were fitted over a k-range from 4 Å⁻¹ to the cut-off imposed by the Zn-edge at 13 Å⁻¹. A k-weighting of 1 was applied throughout most of the analysis. The Cu metal coordination numbers were fixed at the ideal fcc-values to facilitate identification of trends in the remaining XAFS amplitude factors S_0^2 and s_i^2 . This procedure can be justified on the grounds that improvements to the fits were only little above the significance level when the coordination numbers were allowed to vary freely during the fitting analysis. Single-scattering fits obtained by the described procedure are compared to the experimental datasets of samples *I* and *II* in figs. 5.8 and 5.9. Because it was expected that substoichiometric amounts of oxygen in/on the Cu phase might be significant for the state of the catalyst, the k¹-weighted data were also carefully examined for any signs of an oxygen shell. The only statistically significant [92] indication for the presence of oxygen was found for sample *I*, which had been reduced under the mildest of all investigated conditions. Clearly, the reduction of the catalyst does not reach completion at 200°C. It must be pointed out, however, that the Debye-Waller factor and the coordination number information in the oxygen contribution correlated so strongly during refinement that the Debye-Waller factor had to be fixed at 0.04, while the coordination number and shell radius were allowed to float freely during the final fit to the data. Loosening this constraint resulted consistently in unrealistically high coordination numbers and Debye Waller factors. These problems are well known and are commonly encountered when weak EXAFS contributions from a low-Z backscatterer are fitted against a strong

background of higher-Z backscatterers. In principle, better isolation of the oxygen shell information could be achieved by use of, e.g., the ‘difference-file’ technique described in ref. [93], but an implementation of this method has not been available to the author.

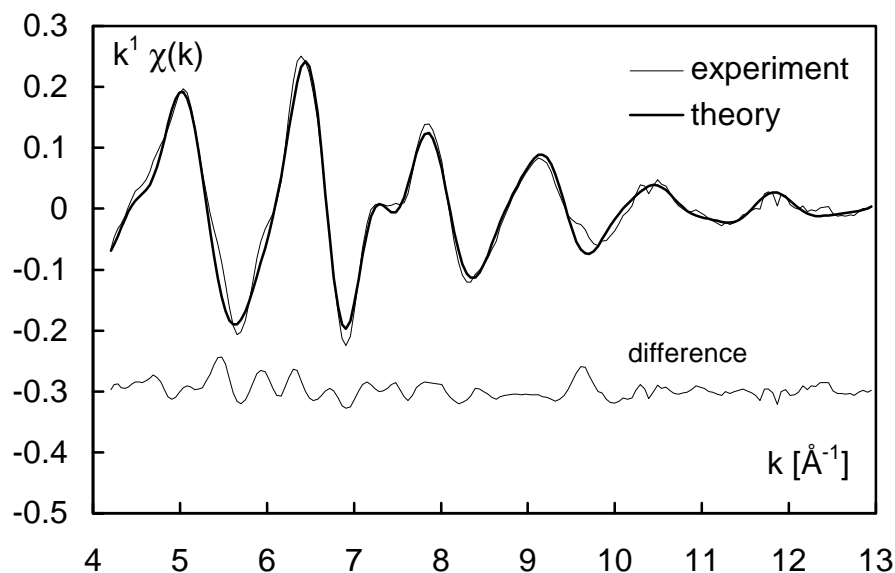


Figure 5.8. Representative six-shell single-scattering fit to the EXAFS data of the reduced catalyst sample denoted I in table 5.2 (partially reduced catalyst; 30 min, 200°C, 5°C/min, 100% H_2).

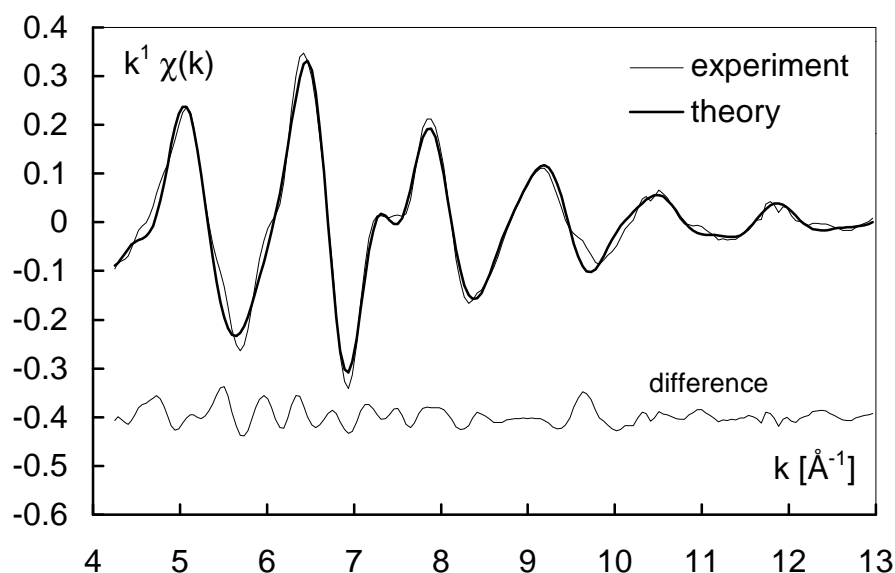


Figure 5.9 Representative five-shell single-scattering fits to the EXAFS data of the reduced catalyst sample denoted II in table 5.2 (5 min, 250°C, 10°C/min, 100% H_2).

Table 5.2. Cu K-edge EXAFS analysis results for the reduction of the calcined Cu/ZnO/Al₂O₃ catalyst precursor as a function of temperature ramp, final reduction temperature and hydrogen partial pressure. Mass flows were in all cases between 60 ml/min and 100 ml/min. *In situ* TEY XAFS measurements were carried out at room temperature under a flow of the reducing gas. Fitted k-ranges were from 4 Å⁻¹ to 13 Å⁻¹ (upper limit imposed by Zn-edge). The listed numbers in brackets give the statistical error estimates for the last given digit of the fitted parameters. The Debye-Waller factors of the fourth coordination shell are artificially enhanced due to a multiple-scattering effect.

<i>Experiment</i>	<i>I</i>	<i>Ia</i>	<i>II</i>	<i>IIa</i>	<i>IIb</i>	<i>III</i>	<i>IV</i>	<i>V</i>	<i>“Cu(OH)₂”</i>	<i>Cu standard</i>
<i>ramp</i>	5°C/min	5°C/min	10°C/min	15°C/min	15°C/min	10°C/min	10°C/min	20°C/min	5°C/min	10°C / min
<i>T_{final}</i>	200°C	250°C	250°C	350°C	500°C	250°C	250°C	250°C	250°C	400°C
<i>t_{dwell}</i>	30 min	30 min	5 min	30 min	30 min	30 min	30 min	5 min	30 min	30 min
<i>gas</i>	100% H ₂	5% H ₂ / He	100% H ₂	100% H ₂	100% H ₂	100% H ₂				
<i>S₀²</i>	0.40 (2)	0.56 (2)	0.59 (2)	0.61 (2)	0.62 (2)	0.63 (2)	0.67 (2)	0.72 (3)	0.71 (3)	0.75 (3)
<i>E_f</i>	-11.3 (4)	-8.7 (4)	-9.6 (4)	-9.3 (4)	-9.4 (4)	-9.6 (4)	-9.5 (4)	-9.5 (4)	-10.1 (4)	-9.9 (4)
<i>N₁ ... N₅</i>										12 / 6 / 24 / 12 / 24 *
<i>R₁ [Å]</i>	2.549 (3)	2.539 (3)	2.539 (3)	2.539 (3)	2.541 (3)	2.537 (3)	2.538 (3)	2.538 (3)	2.543 (3)	2.554 (3)
<i>R₂ [Å]</i>	3.590 (7)	3.569 (7)	3.570 (7)	3.569 (7)	3.572 (7)	3.569 (7)	3.570 (7)	3.570 (7)	3.578 (8)	3.586 (9)
<i>R₃ [Å]</i>	4.470 (7)	4.447 (7)	4.448 (7)	4.446 (7)	4.447 (7)	4.443 (7)	4.445 (7)	4.446 (7)	4.453 (7)	4.467 (7)
<i>R₄ [Å]</i>	4.921 (8)	4.906 (7)	4.907 (7)	4.907 (7)	4.911 (7)	4.908 (7)	4.908 (7)	4.911 (7)	4.918 (7)	4.944 (7)
<i>R₅ [Å]</i>	5.84 (2)	5.79 (1)	5.80 (1)	5.79 (1)	5.79 (1)	5.79 (1)	5.79 (2)	5.79 (1)	5.79 (1)	5.81 (1)
<i>s₁²</i>	0.0176 (8)	0.0171 (7)	0.0171 (7)	0.0169 (8)	0.0166 (8)	0.0166 (7)	0.0170 (7)	0.0165 (7)	0.0167 (8)	0.0154 (8)
<i>s₂²</i>	0.019 (2)	0.020 (2)	0.021 (2)	0.020 (2)	0.020 (2)	0.020 (2)	0.020 (2)	0.020 (2)	0.019 (2)	0.020 (2)
<i>s₃²</i>	0.028 (2)	0.027 (1)	0.026 (1)	0.026 (1)	0.025 (1)	0.025 (1)	0.026 (1)	0.024 (1)	0.023 (1)	0.021 (1)
<i>s₄²</i>	0.016 (2)	0.014 (2)	0.015 (2)	0.014 (2)	0.013 (1)	0.013 (1)	0.014 (1)	0.013 (1)	0.011 (1)	0.010 (1)
<i>s₅²</i>	0.040 (5)	0.035 (4)	0.035 (4)	0.034 (4)	0.033 (4)	0.033 (4)	0.035 (4)	0.034 (4)	0.031 (4)	0.027 (3)
<i>R_O [Å]</i>	1.907 (7)	***	***	***	***	***	***	***	1.92 (3)	***
<i>s_O²</i>	0.04 *	***	***	***	***	***	***	***	0.04 *	***
<i>N_O</i>	4.0 (5)	***	***	***	***	***	***	***	1.0 (3)	***
<i>R-factor**</i>	16.3	17.3	16.5	17.1	17.5	17.0	17.0	16.8	20.0	20.3

*Fixed. **R-factor of fit against raw EXAFS data. ***Below statistical significance level.

Three trends emerge from the EXAFS results summarised in table 5.2. Firstly, the fitted nearest-neighbour distances for all catalyst data are, with the exception of the partially reduced sample (denoted 'I'), somewhat shorter than in the Cu standard. Secondly, the overall amplitude (S_0^2) of the reduced catalysts varies strongly as a function of reduction conditions. Thirdly, the Debye-Waller factors of the reduced catalyst samples are consistently higher than for the Cu standard, especially for the 3rd, 4th and 5th nearest neighbours. The parameters for the reduced, unpromoted Cu precursor ("Cu(OH)₂") are between the values for the reduced catalyst samples and the Cu standard. Except for the variation of the amplitude factor S_0^2 , all parameter changes are rather subtle and quite close to the statistical confidence limits. It must be stressed, however, that they are experimentally reproducible and therefore significant.

Note that the data do not support the previous suggestion [64] that a brass-type alloy with Zn might be formed during reduction of the catalyst precursor. This possibility is very unlikely because doping of significant amounts of Zn into the Cu lattice should result in a detectable fcc-lattice expansion [94], which is clearly not observed.

5.3.2.2. Near-Edge Structure

The multiple-scattering dominated near-edge region is particularly sensitive to changes of the atomic structure in the sample. Its examination adds evidence for the

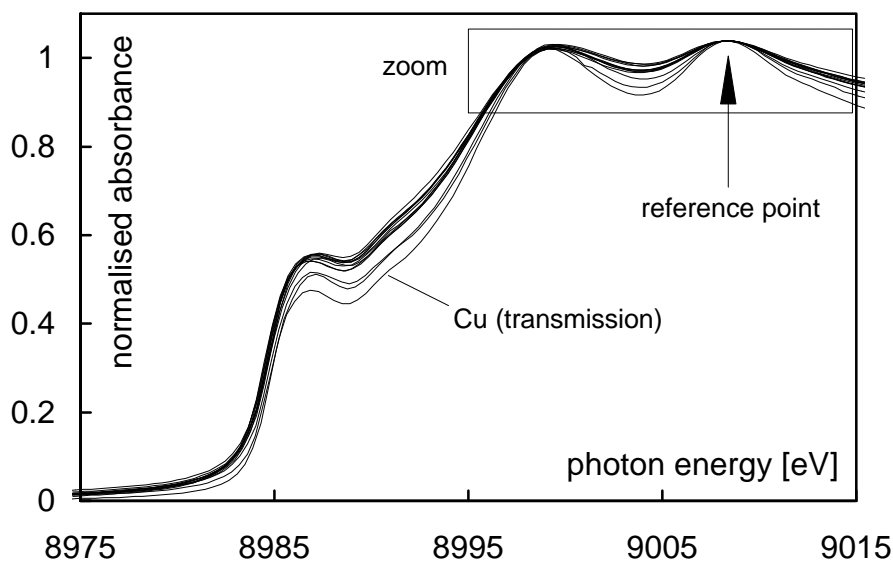


Figure 5.10. Cu K near-edge spectra of the Cu metal standard measured in transmission (lowest spectrum), the TEY Cu metal standard and several of the spectra of the reduced catalyst. The spectra have been aligned at the maximum of the second peak of the near edge structure located at approximately 9008 eV (marked by the arrow as the 'reference point'). The dashed box indicates the window used for the enlarged view in fig. 5.11.

conclusion that the differences observed for the EXAFS functions reflect distinct states of the reduced catalyst. Figure 5.10 contains a collection of normalised X-ray absorption near-edge structure (XANES) spectra, including those of Cu metal standards taken in transmission and TEY mode, of a reduced “Cu(OH)₂” sample, and of the Cu/ZnO/Al₂O₃ catalysts obtained after several different reduction runs. All spectra have been scaled and shifted to align at the maximum of the second XAFS oscillation located at approximately 9008 eV. This point rather than the first edge-step inflection point was used as the reference because the energetic position of the second XANES maximum is less likely to be modified by Fermi level movement or intraatomic electronic transitions.

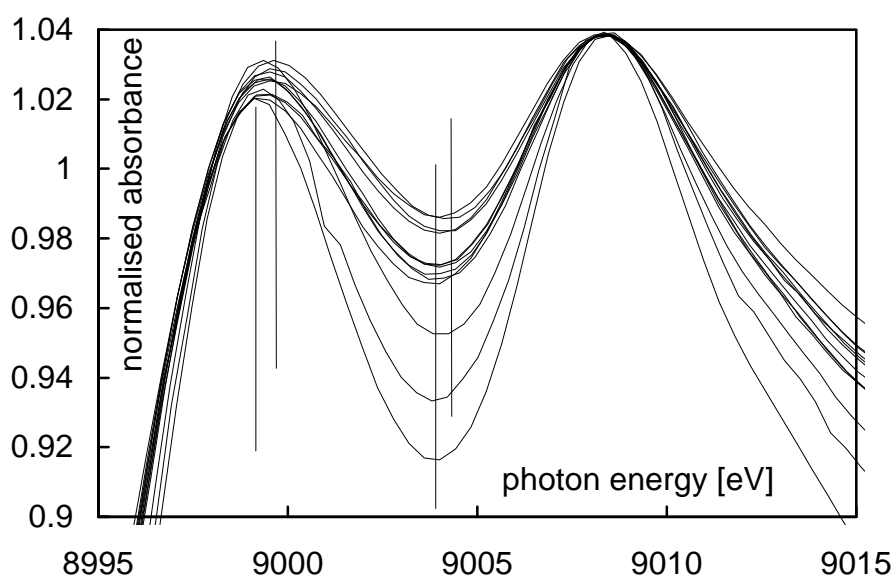


Figure 5.11. Enlarged view of the first two oscillations in the Cu K-edge XAFS spectra presented in fig. 5.10. The vertical bars indicate the largest observed variations of the energetic positions of the peak at 8999 eV and the minimum at 9004 eV.

Compared to the standard transmission spectrum of metallic Cu (lowest spectrum in fig. 5.10), all data exhibit very similar deviations, albeit to a strongly varying degree. On cursory inspection, mainly the overall amplitude loss is evident. A more detailed examination of the spectra reveals more subtle trends which are illustrated by the enlarged view of the first two XAFS oscillations in figure 5.11. It is seen that the positions of the first XAFS maximum and the minimum are slightly shifted in some of the spectra. Most of the changes involve mainly an increase of intensity on the high-energy side of the first peak. *Prima facie*, this intensity gain might simply be taken as evidence for residual oxidation of the Cu component, because one would intuitively expect that some intensity due to dipole-allowed $1s \rightarrow 4p$ transitions (a ‘white line’) in Cu⁺ and/or Cu²⁺ species is present. That this explanation is at least oversimplifying the true situation can be seen by comparison of near-edge data for a

partially and a fully reduced catalyst sample (denoted 'I' and 'Ia' in table 5.2) to the standard spectra for Cu, Cu₂O and CuO (fig. 5.12). While it is seen that the gain of intensity in the spectral region between the first two XANES maxima might indeed be compatible with the presence of CuO or Cu₂O, it is also evident that other deviations between the XANES data of the catalyst and the metallic Cu spectrum cannot be explained with the presence of these oxides. Any significant amount of CuO can be ruled out because its presence should entail the loss of intensity throughout the edge region up to about 8982 eV. In contrast, the opposite, an overall increase of intensity, is seen in the data. The formation of Cu₂O during reduction, previously inferred from X-ray diffraction studies of similar Cu/ZnO catalysts [9,95], cannot be excluded with the same amount of confidence, but the enhanced absorbance of the catalyst in the region between 8980 eV and 8990 eV does not fit the deviations expected from the Cu₂O spectrum either.

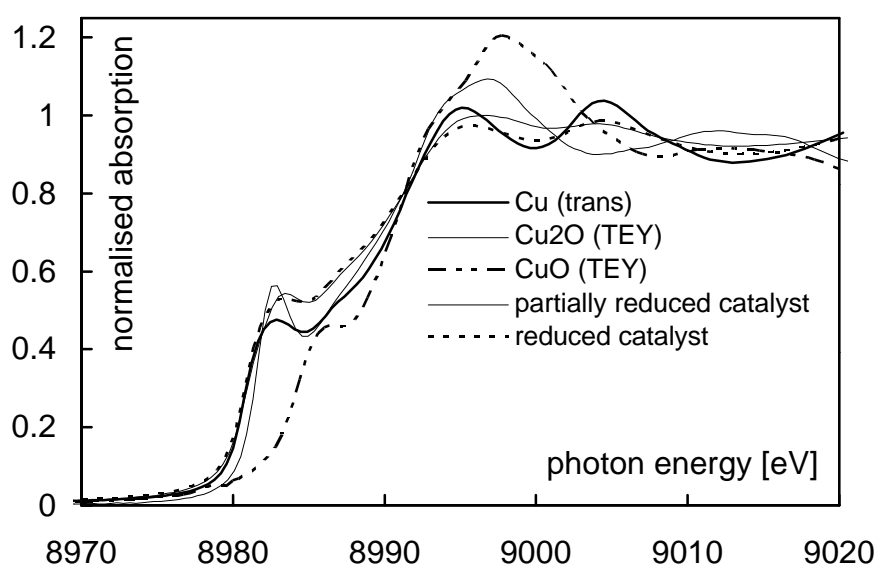


Figure 5.12. Normalised near-edge spectra of Cu (thick full line), Cu₂O (thin broken line) and CuO (thick dot-dashed line) compared to the spectra of a partially and a more thoroughly reduced catalyst sample. The energy scale is referenced to the first edge-step inflection point of the Cu metal K-edge at 8980.3 eV [65,96].

The possibility exists that a non-stoichiometric oxide and/or very small (approximately $< 20 \text{ \AA}$) oxide crystallites are formed, in which case the XANES of the ordered bulk phases would be unrepresentative for the actual oxidic XANES contribution. This possible presence of an amorphous, disordered phase might explain why the distance of the weak nearest-neighbour oxygen shell found by the EXAFS fitting analysis of the partially unreduced sample (1.91 \AA , table 5.2) does neither match the distance expected for CuO (1.96 \AA) nor the value for Cu₂O (1.84 \AA). The principal EXAFS contributions from this sample are characteristic for

zerovalent Cu, but with an approximately 50% lower amplitude than in the bulk metal (table 5.2). The EXAFS amplitude of an oxidic Cu contribution, if present, is almost negligible, suggesting that it is extremely dispersed and/or highly disordered. A more detailed inspection of all Cu K-edge data as a function of treatment conditions sheds some more light on the role of residual oxygen in the reduced material.

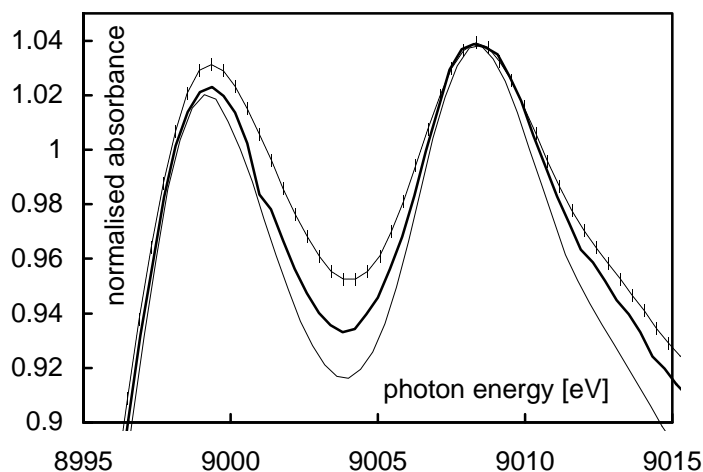


Figure 5.12. Effect of Cu dispersion. Thick full line: TEY Cu standard; thin full line: transmission data for 5 μm thick Cu foil; thin full line with black diamonds: “Cu(OH)₂” precursor reduced at 250°C for 30 min in 100% H₂, heating ramp: 5°C/min.

Figure 5.12 compares the transmission data for a Cu foil to those of the *in situ* reduced TEY powder standard and of the “Cu(OH)₂” precursor. The latter was reduced in 100% H₂ for 30 min at 250°C after applying a temperature ramp of 5°C/min. The data clearly show that the progression from the transmission spectrum, which is representative for the Cu metal bulk structure, to the TEY spectrum of the *in situ* H₂-treated (T = 400°C) macroscopic powder (particle sizes about 1 μm) and then to the microcrystalline (particle diameters approximately 450 Å, derived from XRD LBA with the Scherrer equation) sample of the *in situ* reduced ‘Cu(OH)₂’ precursor is accompanied by (i) an increase of the height of the first peak and (ii) by added intensity on its high energy side. This apparent dependence of the spectra on the dispersion of the pure metal indicates that a near-surface effect could play a rôle in the modification of the XAFS. This suggestion should not be taken to imply that the smaller XAFS amplitudes in the powdered samples reflect reduced coordination numbers of surface atoms [97]. This possibility can be ruled out because the XRD-derived particle sizes are far too large to be compatible with this interpretation. It seems rather more likely that the presence of enhanced disorder and/or the formation of a quasi-amorphous oxide phase in the near-surface region of the sample explains

the amplitude variations. In this view, the apparent correlation of the amplitude deviations with particle size could be due to the larger fraction of the near-surface volume in smaller particles. The existence of an oxidic Cu phase would be remarkable, as both powdered Cu samples had been treated in H₂ at 300°C - 400°C prior to the measurements. These temperatures are well above the point at which bulk reduction of CuO and Cu₂O occurs. This raises the possibility that hitherto unidentified subsurface and near-surface oxygen species, possibly analogous to those recently found in Ag lattices [98-101], could be responsible for the observed effects (*vide infra*).

The influence of reduction conditions on the near-edge XAFS of the catalyst is illustrated by the spectra in figure 5.13. The data show that increasingly vigorous reduction conditions (higher temperatures, higher partial pressures of H₂, longer total reduction times, faster temperature ramps) tend to produce a more metal-like near-edge spectrum. This trend matches the variations of the S_0^2 amplitude results from the EXAFS fitting analysis (table 5.2).

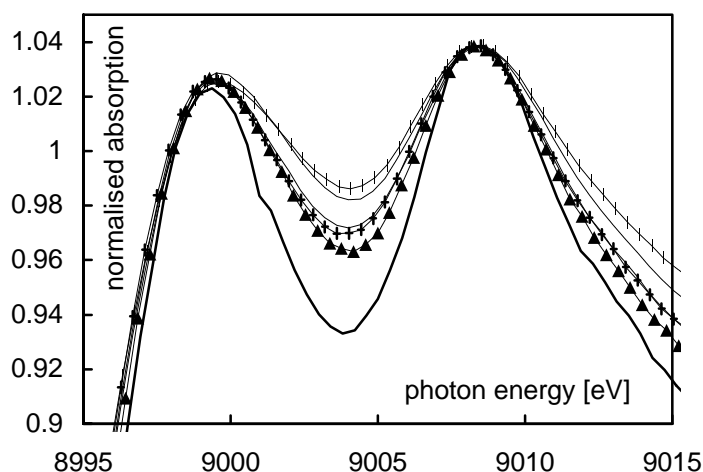


Figure 5.13. Effect of reduction conditions. Spectra from top to bottom (code in table 5.2 in brackets): thin line with black diamonds: catalyst reduced for 30 min at 250°C in 100% H₂, ramp. 5°C/min (*Ia*). Thin broken line: catalyst reduced for 5 min at 250°C in 100% H₂, ramp. 10°C/min (*II*). Thin full line: catalyst reduced for 30 min at 250°C in 5% H₂, ramp 10°C/min (*III*). Thin full line with crosses: catalyst reduced for 30 min at 250°C in 100% H₂, ramp 10°C/min (*IV*). Broken thin line with filled triangles: catalyst reduced for 5 min at 250°C in 100% H₂, ramp 20°C/min (*V*). Thick full line: TEY Cu standard.

Note, however, that none of the near-edge data match the spectrum of the TEY Cu standard, even in the case of spectrum '*V*' which exhibits, within confidence limits, the same value for S_0^2 as the Cu metal standard measured by TEY detection (cf. table 5.2). The reason for the persistent amplitude reductions are the larger Debye-

Waller factors, the influence of which is particularly strong in the near-edge multiple-scattering regime (additivity of the thermal dephasing effects of each scattering event). This suggests either that some form of disorder is important in determining the amplitude behaviour of the Cu phase, or that the average size of the metallic particles is very small.

Lattice order in the Cu particles would be expected to improve on increasing the reduction temperature. Figure 5.14. presents the results obtained by annealing a previously mildly reduced sample (sample ' in table 5.2, thin broken line in fig. 5.13) further in H₂. It is seen that the peak height ratio of the annealed material does indeed begin to approach that of pure Cu. This, a very weak trend in the fitted EXAFS parameters towards a higher amplitude, and lower Debye-Waller factors (spectra 'IIa' and 'IIb' in table 5.2) support the expectation that lattice order increases during high-temperature treatments. However, the EXAFS changes observed on annealing are nevertheless almost negligibly small. The XAFS amplitude is substantially reduced even after a treatment at 500°C. A factor other than lattice ordering must therefore contribute to the reduced XAFS amplitudes of the catalyst.

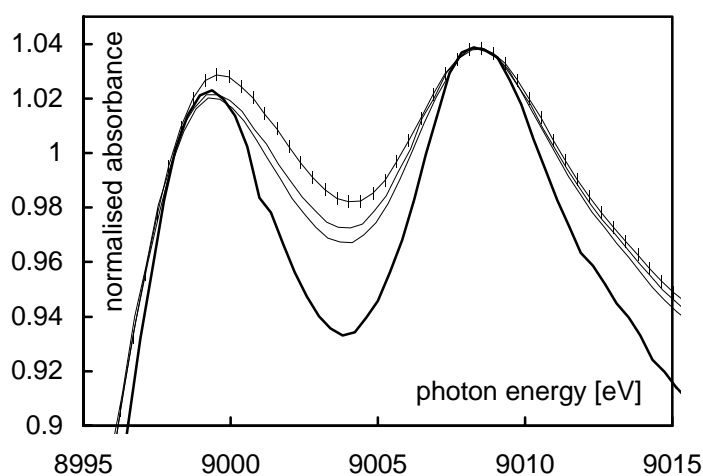


Figure 5.14. Effect of annealing on the reduced catalyst. Thick full line: TEY Cu standard; thin full line with black diamonds: catalyst reduced for 5 min at 250°C in 100% H₂, ramp. 10°C/min; thin broken line: the same sample heated to 350°C with a temperature ramp of 15°C/min and held at the final temperature for 30 min. Thin full line: the same sample further heat-treated for 5 min at 500°C with a ramp of 15°C/min. The catalyst spectra correspond to samples II, IIa, and IIb in table 5.2.

As mentioned above, a more obvious explanation could invoke the presence of very small particle sizes, as a large number of partially uncoordinated surface atoms would lead to a reduction of the observed coordination numbers. However, the examination of the spectra obtained for the partially unreduced sample as well as the

data for pure Cu samples have also raised the possibility that residual oxidation might be responsible for the observed amplitude reductions.

The latter possibility was therefore addressed by exposing a reduced sample at room temperature to an amount of air below the exposure limit for bulk oxidation of Cu. The spectrum obtained after dosing $10^8 \pm 25\%$ L (1 L = 10^{-6} torr s) of oxygen at a partial pressure of 0.2 atm onto a sample of the reduced catalyst is presented in figure 5.15. It is seen that the oxygen exposure induces strikingly similar spectral changes as those observed as a function of reduction conditions and annealing (cf. figs. 5.13. and 5.14.). Moreover, subsequent re-reduction of the air-exposed sample proves possible, and reveals that the oxygen-induced changes to the catalyst morphology are fully reversible (fig. 5.15). These conclusions do also correlate well with the results of a curve-fitting analysis of the corresponding EXAFS functions (table 5.3): only the amplitude parameter $S\sigma^2$ decreases and increases by $13\% \pm 5\%$ during oxidation and re-reduction. Interestingly, the R-factor of the oxygen-exposed sample improves significantly upon including a weak oxygen shell at 1.87 ± 0.01 Å in the fit (as for the partially unreduced sample, however, the Debye-Waller factor had to be fixed at 0.04 to obtain a physically sensible result). All other parameters are, within the confidence limits, unaffected by the XAFS changes.

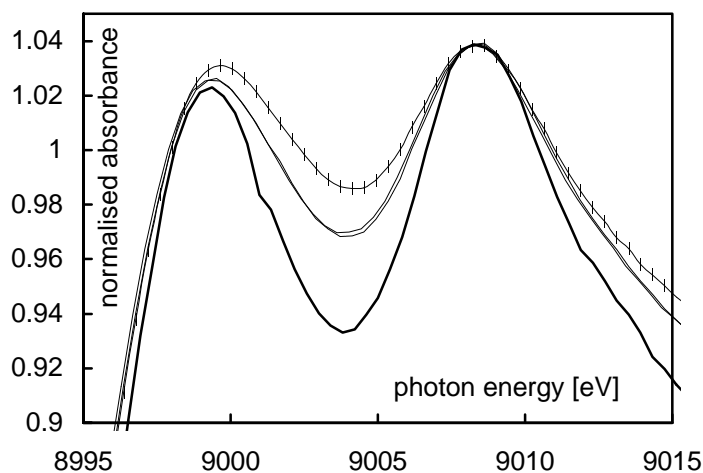


Figure 5.15. Effect of small O₂ exposure on the reduced catalyst. Thick full line: TEY Cu standard; thin full line: catalyst reduced for 30 min at 250°C in 100% H₂, ramp. 10°C/min; thin full line with black diamonds: catalyst subsequently exposed to 10⁸ L of O₂.

These results demonstrate clearly that the oxygen content of the catalyst is a critical factor in the determination of its morphology. The effect of oxygen does not become evident as a separate ordered phase or a Debye-Waller-type damping of the metal

XAFS. It appears as if exposure to oxygen leads to a reversible removal of Cu from the metallic Cu phase.

Table 5.3. EXCURV92 fitting analysis for the EXAFS data corresponding to the spectra given in figure 5.15.

	reduced catalyst	after exposure to 10 ⁸ L O ₂	re-reduced catalyst	TEY Cu standard
S_0^2	0.67 (2)	0.58 (2)	0.66 (2)	0.75 (3)
E_f [eV]	-9.5 (4)	-10.1 (4)	-10.1 (4)	-9.9 (4)
$N_1 \dots N_5$		12 / 6 / 24 / 12 / 24 **		
R_1 [Å]	2.538 (3)	2.540 (3)	2.539 (3)	2.554 (3)
R_2 [Å]	3.570 (7)	3.572 (7)	3.572 (7)	3.586 (9)
R_3 [Å]	4.445 (7)	4.449 (7)	4.448 (7)	4.467 (7)
R_4 [Å]	4.908 (7)	4.912 (1)	4.912 (7)	4.944 (7)
R_5 [Å]	5.79 (2)	5.80 (1)	5.80 (1)	5.81 (1)
s_1^2	0.0170 (7)	0.0170 (1)	0.0169 (7)	0.0154 (8)
s_2^2	0.020 (2)	0.020 (2)	0.020 (2)	0.020 (2)
s_3^2	0.026 (1)	0.026 (1)	0.025 (1)	0.021 (1)
s_4^2	0.014 (1)	0.014 (1)	0.013 (1)	0.010 (1)
s_5^2	0.035 (4)	0.034 (4)	0.034 (4)	0.027 (3)
N_O	-	0.7 (1)	-	-
R_O [Å]	-	1.87 (1)	-	-
s_O^2	-	0.04**	-	-
k -range [Å ⁻¹]	3 - 13	3 - 13	3 - 13	3 - 13
R -factor	17.0 (17.2*)	16.9 (19.0*)	17.3 (17.5*)	20.3

*R-factor obtained when oxygen shell is not included in fitting analysis. ** Fixed values.

Several mechanisms could explain the remarkable influence of oxygen on the Cu XAFS:

Formation of a highly disordered, separate oxide phase - The reaction between oxygen and the Cu particles is expected to be exothermic. As exposure to oxygen occurred at a partial pressure of 0.2 atm, it is possible that local heating of the particles resulted in reaction conditions far from thermodynamic equilibrium. These conditions could favour the formation of extremely small, disordered oxide particles which would not exhibit significant XAFS contributions. Reduction of this amorphous phase would release dispersed Cu which could migrate back to the Cu particles of the catalyst.

Dissolution of oxygen in the Cu lattice - It has long been known that oxidic layers formed on single crystalline Cu in the exposure range of the dosing/re-reduction experiment (fig. 5.15) contain oxygen in amounts equivalent to stoichiometric oxide layers less than a few Å thick [102,103]. UHV studies indicate that, depending on the crystal face, exposures of more than $10^6 - 10^9$ L of O₂ are necessary to observe the onset of bulk oxide formation at room temperature [104-106]. Exposure to lower amounts ($< 10^4$ L) of oxygen results only in chemisorbed species. Interestingly, after saturation of the surface with adsorbed oxygen, a so-called 'induction period' is often observed in the pressure range between 10^4 L and 10^6 L, *i.e.* it appears that any further interaction with oxygen does not affect the surface properties of the O-covered Cu surfaces. This suggests that processes occur in the subsurface region of Cu which are an essential prelude to the final bulk oxidation process. It is possible that the subsurface oxygen species formed in the intermediate exposure range is/are responsible for the changes observed by TEY XAFS.

This mechanism would require that the XAFS amplitude is reduced through a Debye-Waller-type dephasing effect of mobile subsurface/interstitial oxygen species. As mentioned above, the presence of such dissolved, active lattice oxygen is well established for Ag surfaces [98-101]. It seems therefore reasonable to consider their presence also in the case of Cu metal. If the thermal mobility of these species was high enough, their effect on the XAFS could essentially be the observed loss of amplitude *via* dephasing of the scattered photoelectron wave. However, an important difference between the two metals renders this theory somewhat unlikely: the smaller lattice constant of Cu (3.61 Å vs. 4.09 Å in Ag) is expected to be an efficient barrier to dissolution and should impair the mobility of any oxygen species in the lattice. Furthermore, it is difficult to see how the presumably small concentration of oxygen (typical interstitial site occupancies for oxygen dissolved in bulk Ag are 0.01% [98]) could induce amplitude changes of 10% and more.

However, any penetration of the Cu lattice by larger amounts of oxygen would be accompanied by lattice disruption. It is therefore possible that a disruption of the Cu surface structure destroys pair correlations *via* amorphisation of the outer atomic layer of the particles. Again this would be compatible with the XAFS results, but it is difficult to see why the effect should not be visible as a change of the Debye-Waller factors.

Dynamic particle restructuring - The amplitude variations observed as a function of reduction and oxidation conditions are rather reminiscent of the amplitude changes observed by Clausen *et al.* who varied the oxidation potential of the gas phase over

Cu/ZnO catalysts [37]. They observed XAFS amplitude changes which they interpreted as evidence for changes of the particle shapes due to wetting/non-wetting of the ZnO support. This interpretation appeared to be in line with an argument based on thermodynamics [107] invoking the surface free-energy of the contact plane between particles and support. It was argued that reducing conditions would result in the formation of a more metal-like, oxygen-deficient ZnO surface which would be more wettable by adsorbed Cu. In this view, reducing conditions should lead to lower XAFS amplitudes, as the more two-dimensional spreading of Cu would increase the number of surface atoms. Oxidation of the ZnO surface should result in the formation of three-dimensional crystallites.

The opposite was observed in the present study. Oxidation of the catalyst sample results in the loss of XAFS amplitude, whereas reduction induces higher XAFS amplitude indicative for ‘balling up’ of the Cu particles. Taking the idea of surface free energy effects a little bit further, it could be argued that oxidation of the Cu particle surfaces could also increase the affinity between the particle surface and the oxide support - as if the rôles of support and adsorbate were the reverse of those in the catalyst studied by Clausen *et al.* [37]. Note also, that the catalyst studied here had a Cu content which exceeded that of ZnO by a large margin, whereas Clausen *et al.*’s material contained ZnO in excess. Only a fraction of the total Cu content would therefore be expected to ‘wet’ the ZnO component in the present catalyst.

It is interesting to note that recent SEXAFS data for Cu adsorbed on a single-crystalline Al₂O₃ substrate have shown that pre-oxidation of the surface induced enhanced wetting by the Cu adsorbate [108]. On the contrary, pre-reduction of the Al₂O₃ support resulted in three-dimensional crystallites. It therefore appears that Clausen *et al.*’s theory invoking surface free energy differences at the particle-support contact plane [37] might be oversimplifying the mechanism which determines the particle shapes and, ultimately, the dispersion of the Cu phase.

5.3.2.3. Line-Broadening Analysis of XRD Data: The Influence of Surface Atoms

To assess the influence of surface atoms on the XAFS amplitude reductions, a particle size analysis was carried out by XRD. The FWHM linewidths of the most intense reflections in the *in situ* X-ray diffraction pattern of two reduced samples were first analysed by use of the Scherrer equation (5.1). For the ZnO component, the broadening of all lines located between 2Θ values of 30° and 60° (cf. fig. 5.4) indicated consistently lattice order on a scale of $80 \text{ \AA} \pm 5 \text{ \AA}$. In contrast, the Scherrer LBA of the (111) and (220) reflections of Cu gave quite different results. It suggested

particle sizes on the order of 80 Å for the Cu(111) plane, while the broadening of Cu(220) line indicated order on a scale of 57 Å. The apparent discrepancy between these results could be removed by careful fitting of the diffraction pattern and performing a full LBA [79] of the Cu(111) line. The result now indicated an average particle size of approximately 50 Å (fig. 5.16), and was in good agreement with the Scherrer analysis of the (220) reflection. The pattern fitting revealed that the difference between the results of the two LBA approaches arises because a large fraction of the Cu(111) intensity resides in long ‘tails’ on both flanks of the diffraction line which stretches over a 2Θ range of a few degrees. The lineshape of the pseudo-Voigt function used for the determination of the FWHM was therefore inappropriate for the analysis of the Cu(111) reflection.

A simple 2-parameter function ($D^a \cdot \exp(-D/b)$), where D is the particle diameter) was fitted to the LBA results (best parameters: $a = 1.23$, $b = 25.3$ Å) and the total fraction of Cu surface atoms in the sample was calculated by modelling the Cu particles as homogeneous spheres, with the fraction of surface atoms given by the ratio between the volume of the outer shell of thickness d (where $d = 2.56$ Å, the diameter of a Cu atom) and the total volume of the sphere (right diagram of fig. 5.16). The result of this calculation was a surface atom fraction of 37%. The magnitude of the XAFS amplitude change per surface atom is 25% for the first coordination shell of a (111)-like surface atom. This suggests that amplitude reductions of the order of $0.37 \times 0.25 \approx 10\%$ are expected.

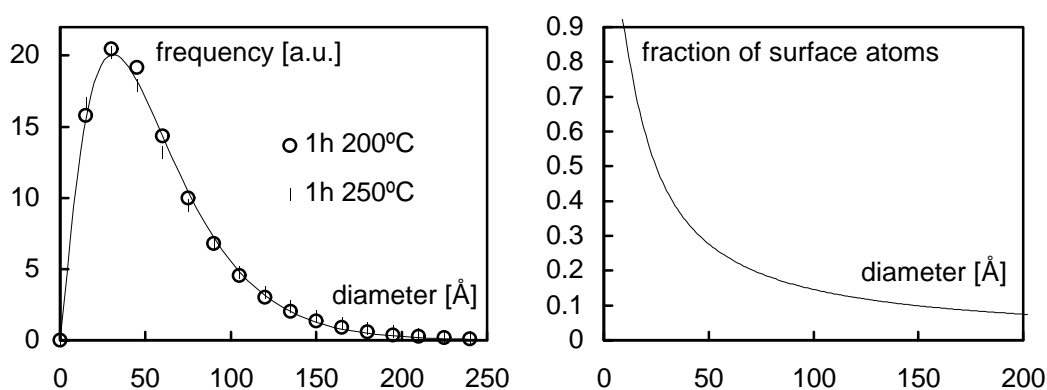


Figure 5.16. Left diagram: Results of line-broadening analyses using the Cu(111) reflection of the reduced catalyst. The full line represents the fitted 2-parameter function described in the text. Open circles: data for catalyst reduced for 1h in 5% H₂/He at 200°C. Filled circles: catalyst reduced for 1h in 5% H₂/He at 250°C. Right diagram: fraction of Cu surface atoms in dependence on Cu particle diameter assuming structureless spherical particles with the fraction of surface atoms given by the volume of the outer shell with the thickness of the atomic diameter of Cu.

Note that this calculation is likely to underestimate the actual XAFS amplitude reductions. Problems arise for two reasons: firstly, modelling the particles as structureless spheres becomes inappropriate for sizes below approximately 50 Å because the average coordination number of a surface atom in a small particle is actually lower than predicted by the volume ratios. The expected discrepancies are illustrated in the left diagram in fig. 5.17, which compares surface atom fractions calculate with the simple model with those predicted by a molecular dynamics simulation of Cu particles. Secondly, the present calculation neglects the effect of anharmonic movement of the surface atoms. This effect is particularly strong in Cu [73] and introduces an asymmetry into the pair distribution function which results in apparently lowered coordination numbers. The graphs on the right diagram of fig. 5.17. allow an assessment of the influence of this effect on the present analysis results.

The XRD-derived particle sizes thus suggest that lower coordination around surface atoms is likely to contribute to the XAFS amplitude reductions. The LBA indicates that amplitude reductions of more than 10% are expected under the reduction conditions employed during the two *in situ* XRD experiments. The XAFS dataset which is most representative for the XRD result is that of sample 'III' (cf. table 5.2). It exhibits an amplitude reduction of $16\% \pm 7\%$ (equivalent to a first shell coordination number of approximately 10.2) relative to the TEY Cu standard.

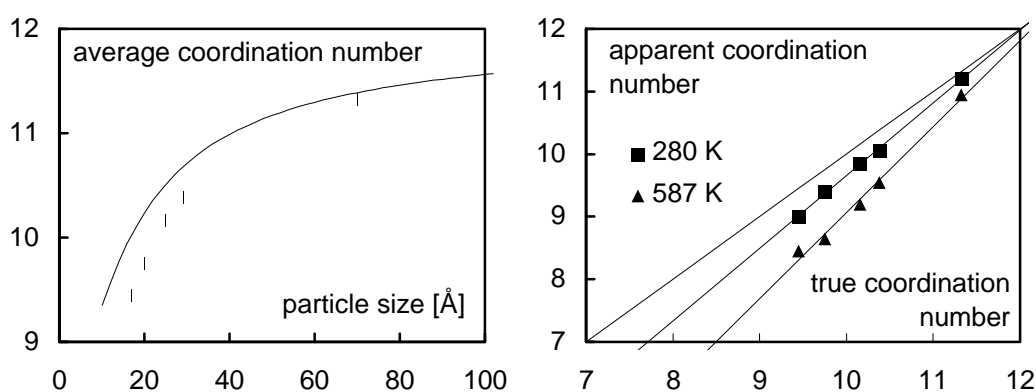


Figure 5.17. Effect of anharmonic movement of the surface atoms on the EXAFS of small Cu clusters. Left diagram: results of molecular dynamics simulations for the correlation between particle size and average first-shell coordination number in Cu clusters containing 256 (cluster diameter: 17 Å) to 16727 (cluster diameter: 70 Å) atoms (black diamonds); the line represents the coordination numbers expected from a surface-to-bulk volume model assuming structureless spheres and a coordination number of 9 at the surface. Right diagram: errors expected for a standard EXAFS analysis including best-fit Debye-Waller factors if no account is taken of the non-Gaussian pair distributions due to anharmonic movement. All molecular dynamics results taken from [72-74]).

Other features in the EXAFS fitting results add support to an interpretation in terms of very small particle sizes. Firstly, all Debye-Waller factors obtained for the samples are significantly increased relative to the bulk values. Furthermore, the differences to the bulk values increase as a function of coordination shell distance - a clear indicator for decreasing pair correlations to more distant shells. Another interesting deviation from the bulk Cu parameters is seen for the coordination shell distances. They are somewhat shorter (by approximately 0.01 Å) than expected for a Cu metal lattice (cf. tables 5.2 and 5.3). Again this difference can be explained by invoking the anharmonic contribution to the thermal vibrations, which has been shown to result in an apparent contraction of the nearest neighbour distances when the standard EXAFS analysis is applied to very small particles [91].

5.3.2.4. X-ray Absorption Near-Edge Structure Calculations for Small Cu Clusters: The Rôle of Long Range Order

To allow an assessment of the experimentally observed changes in the XANES features, *ab initio* calculations of the near-edge structure of Cu clusters as a function of cluster size have been performed. The curved-wave multiple-scattering (MS) code FEFF6.01 [109] was employed for these calculations. Due to restrictions in the executable version of FEFF6 available at the time, only the XAFS of very elementary clusters have been evaluated (a more extensive analysis is currently under investigation by the author in consultation with Professor J.J. Rehr). The calculations were carried out including all possible scattering paths up to a length of 13 Å, setting the FEFF-parameter R_{max} to 6.5 Å. The highest order of possible MS events included in the calculations thus corresponds to 5. All scattering paths which contributed with an XAFS amplitude of less than 4% of the most intense path were omitted from the analysis (it has been checked that this simplification, while speeding up the calculations substantially, bears no significant relevance for the final result). A correlated Debye model [110-112] was employed to derive Debye-Waller factors (the Debye temperature of Cu was assumed to be 315 K [113]). It has previously been shown that the MS expansion implemented in FEFF6, when used entirely unrestricted, yields results which converge very well with experimental data and the results of elaborate band structure calculations [109]. For the present FEFF6 analysis, the number of included scattering paths was substantially smaller than in an unrestricted calculation, but the results are remarkably similar to those obtained by the more full-fledged evaluations presented in ref. [109].

The results clearly illustrate how sensitively the near-edge structure of Cu responds to changes of the coordination in the first six shells (fig. 5.18). The calculated spectra

are in excellent agreement with SEXAFS and EXAFS data of small Cu clusters adsorbed on a single crystalline Al₂O₃(0001) surface [108], on SiO₂ [114] and on dispersed Al₂O₃ [63]. They also match trends seen in data for very small Cu clusters supported in a noble gas matrix [45] and for thin Cu films supported on a W(111) surface [115].

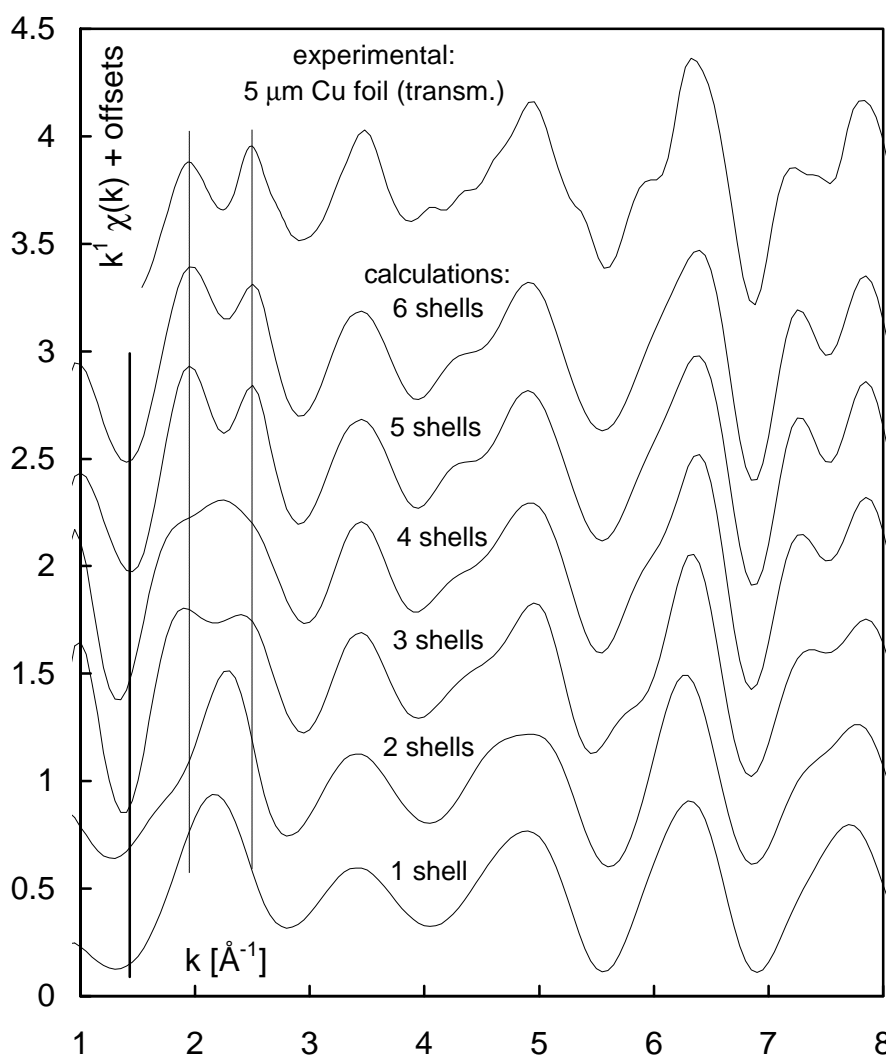


Figure 5.18. XAFS functions of Cu as a function of cluster size. The upper spectrum has been determined experimentally in transmission mode using a 5 μm Cu foil. The lower six spectra illustrate (from bottom to top) the progression from a Cu cluster with one nearest-neighbour distance to a cluster with six nearest neighbours.

The interpretation of the XANES in the experimental data focused on the ‘double-peak’ fingerprint in the XAFS of Cu at about $k \approx 2.2 \text{ \AA}^{-1}$. The calculations reveal that this feature is obtained first when the fcc-cluster around the absorber atom contains at least five nearest neighbour shells. Agreement with experimental data for bulk Cu is nevertheless poor. It improves somewhat by including a sixth coordination shell

(larger clusters are currently under investigation), but is still not correct. Interestingly, the relative intensity of the two XANES features is not reproduced satisfactorily even when the first 23 shells are included in the FEFF calculation (cf. ref. [109]). Agreement with the experimentally determined intensities is only evident after a full MS analysis including 31 shells has been performed [109].

It is worth pointing out that the observation of the ‘double-peak’ XANES structure in clusters with five and six shells is incompatible with a recent interpretation of this feature given by Rehr and co-workers [109]. They concluded from the analysis of calculations including the first 31 shells that interference between the single-scattering contributions from the 3rd and 7th shell in the Cu lattice is responsible for the depression between the two near-edge peaks [109]. In view of the fact that the small-cluster calculations reproduce the feature in *the absence of the 7th shell* (fig. 5.18) this interpretation has to be reviewed. Some caution not to over-interpret the small-cluster results may be advisable because the exclusion of higher order MS paths and coordination shells might have lead to fortuitous agreement between the calculated and the experimental results. Given the complex set of scattering paths underlying the XANES calculation, however, this seems an unlikely event. The good match between the energetic positions of the peaks in the calculated and the experimental spectrum, as well as the remarkable agreement with the results for a 23-shell cluster [109] suggest that the ‘double peak’ is intrinsic to multiple scattering effects in the close vicinity of the central atom. Following consultation with Prof. J.J. Rehr, work with an unrestricted FEFF6 code is currently being carried

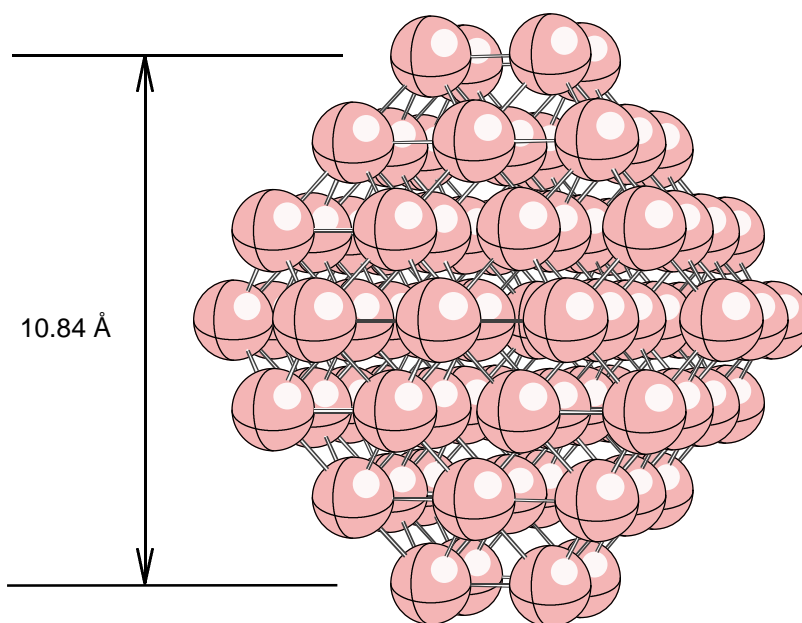


Figure 5.19. Minimum size Cu fcc-cluster required for the central atom to exhibit the ‘double-peak’ near-edge feature characteristic of the Cu metal XAFS.

out by the author to settle this point.

The most interesting result of the FEFF analysis is therefore the observation that the calculated XANES spectra of small clusters exhibit distortions from a bulk-Cu spectrum which seem to match those in the experimental spectra of the Cu component in the catalyst. It is remarkable that the XANES calculations indicate that good lattice order throughout the first 20 - 30 coordination shells is necessary to obtain the near-edge spectrum of Cu metal. To provide an impression of the short-range order required around a Cu absorber to exhibit at least the metal-like 'split' XANES structure, a ball-and-stick model of the 5-shell cluster is drawn in figure 5.19. The cluster contains 79 atoms and its diameter is approximately 11 Å. For comparison, the cluster including 30 coordination shells has a diameter of approximately 24 Å [109]. This suggests that the XANES changes observed in the catalyst data might originate in lattice distortions on a distance scale which is not probed by the EXAFS.

5.3.2.5. Interaction of the Reduced Catalyst with CO₂

A previous TEY XAFS study [61] suggested the reduced catalyst could be oxidised by exposure to CO₂ at the methanol synthesis temperature. This experiment was repeated in detail. A reduced sample of the catalyst was exposed to a mixture of 10% CO₂ in He at 250°C. The resulting XAFS is identical to that of the reduced catalyst. This is most clearly indicated by an examination of the characteristic XANES features (fig. 5.20). In line with this, the analysis of the extended fine-structure did not reveal any differences between the spectra.

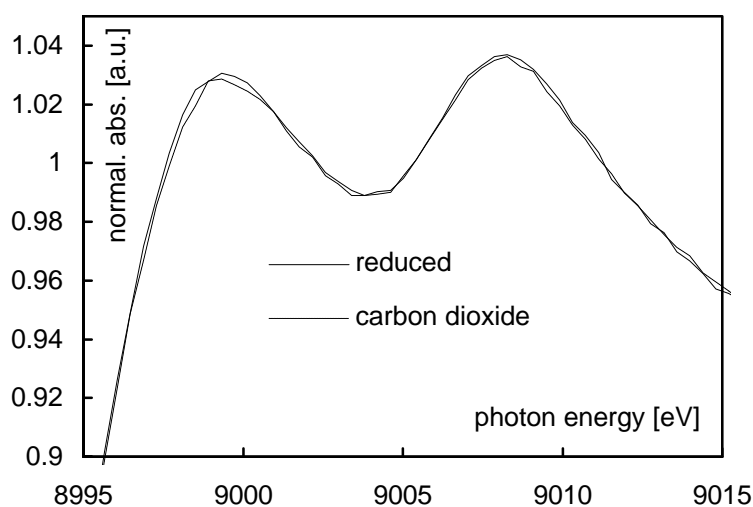


Figure 5.20. Near-edge data of a reduced, CO₂-exposed, and a N₂O-exposed catalyst sample.

Further investigations of the conditions under which CO₂ might oxidise the Cu particles revealed that the presence of small air contaminations in the CO₂/He mixture could result in the formation of the Cu₂O phase observed in the previous study. It must therefore be concluded that the nearest-neighbour oxygen shell which had been interpreted as adsorbed oxygen [61] was a Cu₂O skin formed by oxygen exposure of the reduced material.

5.3.2.6. State of the Catalyst under Synthesis Conditions: TEY Measurements at Elevated Pressure

These experiments investigated for the first time the possibility of performing TEY XAFS measurements at elevated pressures. They addressed the state of the catalyst surface under synthesis conditions. A catalyst sample was reduced in H₂ (sample 'V' in table 5.2) and subsequently exposed to synthesis gas (1% CO, 1% CO₂, 8% H₂, remainder He) at 250°C under increasing pressure. XAFS data were obtained for pressures up to 40 atm. The k¹-weighted raw EXAFS functions obtained from these data are given in figure 5.21.

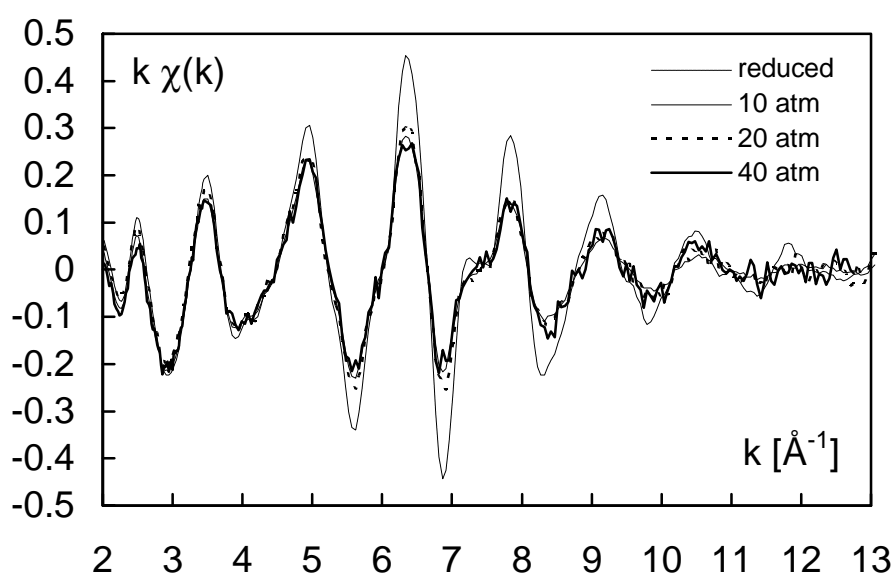


Figure 5.21. Unfiltered, k¹-weighted EXAFS functions for the reduced (dashed line) catalyst and the same sample exposed to syngas at three different pressures.

The results of the extended fine-structure analysis are listed in table 5.4. Significant changes of the fit parameters are seen only for the Debye-Waller factors, which are, due to the elevated temperature, much larger than for the Cu standard and the reduced catalyst at room temperature. Some deviations in the amplitude parameters appear to present in the spectrum obtained at a pressure of 40 atm. However, the

fitting result to this spectrum exhibited also worst agreement with experiment. This result is readily understood in view of the comparatively poor signal-to-noise quality of this dataset (fig. 5.21). The changes observed in the EXAFS fits appear to be negligible.

Table 5.4. EXAFS analysis results for the catalyst sample exposed to syngas at elevated pressures.

	reduced catalyst T = 298 K	syngas 10 atm T = 548 K	syngas 20 atm T = 548 K	syngas 40 atm T = 548 K	TEY Cu standard T = 298 K
S_0^2	0.72 (3)	0.66 (2)	0.66 (3)	0.55 (3)	0.75 (3)
E_f [eV]	-9.5 (4)	-8.3 (4)	-8.3 (5)	-8.5 (6)	-9.9 (4)
$N_1 \dots N_5$	12 / 6 / 24 / 12 / 24 **				
R_1 [Å]	2.538 (3)	2.528 (3)	2.528 (4)	2.529 (4)	2.554 (3)
R_2 [Å]	3.570 (7)	3.559 (7)	3.553 (9)	3.57 (1)	3.586 (9)
R_3 [Å]	4.446 (7)	4.456 (8)	4.45 (1)	4.45 (1)	4.467 (7)
R_4 [Å]	4.911 (7)	4.882 (7)	4.89 (1)	4.89 (1)	4.944 (7)
R_5 [Å]	5.79 (1)	5.81 (2)	5.81 (2)	5.84 (5)	5.81 (1)
s_1^2	0.0165 (7)	0.0253 (8)	0.024 (1)	0.021 (1)	0.0154 (8)
s_2^2	0.020 (2)	0.028 (2)	0.026 (2)	0.023 (3)	0.020 (2)
s_3^2	0.024 (1)	0.042 (2)	0.038 (2)	0.036 (3)	0.021 (1)
s_4^2	0.013 (1)	0.024 (2)	0.024 (3)	0.020 (3)	0.010 (1)
s_5^2	0.034 (4)	0.049 (5)	0.045 (6)	0.057 (2)	0.027 (3)
k -range [Å ⁻¹]	3 - 13	3 - 13	3 - 13	3 - 13	3 - 13
R -factor	16.8	15.3	20.4	24.8	20.3

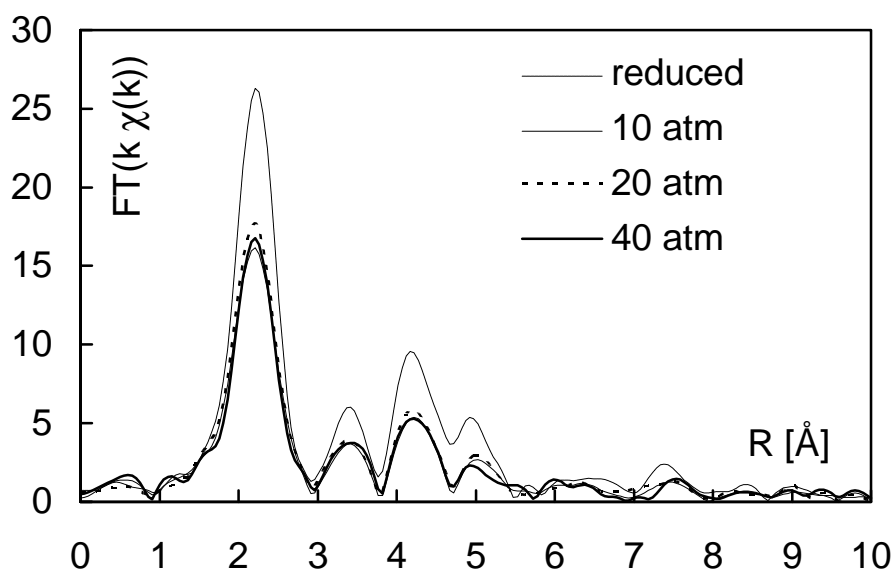


Figure 5.22. Fourier transforms of the EXAFS functions presented in fig. 5.17. k -window: $3 \text{ \AA}^{-1} - 13 \text{ \AA}^{-1}$.

The same conclusion is borne out by an inspection of the near-edge region of the data (fig. 5.23). Within the signal-to-noise ratio of the spectra, no significant changes are discernible as a function of synthesis gas pressure. The Cu phase probed by the XAFS is essentially in a metallic state.

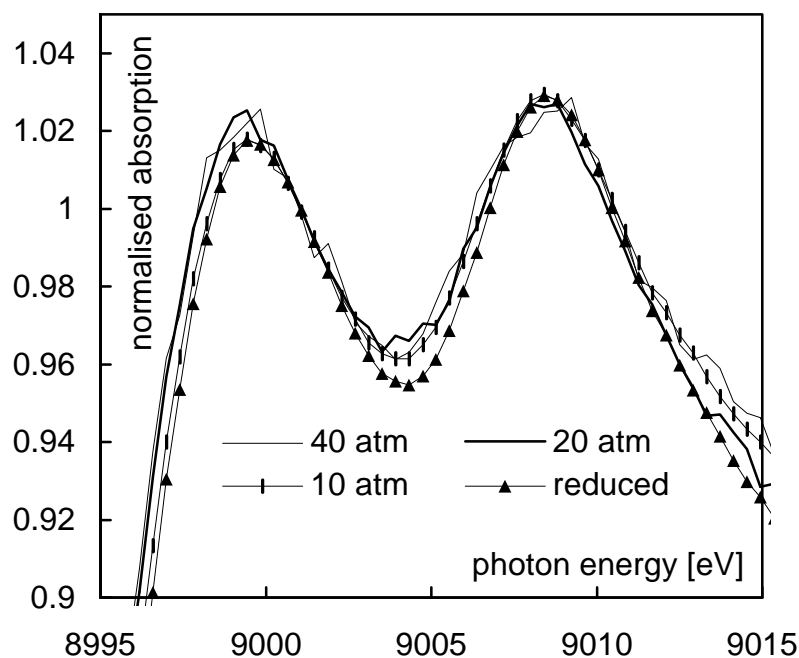


Figure 5.23. Near-edge oscillations in the XAFS data for the reduced catalyst (filled triangles) and the same sample subsequently exposed to increasing pressures of a synthesis gas mixture (see inset for assignments).

5.4. Summary

The combined XAFS/XRD investigations of the Cu/ZnO/Al₂O₃ catalyst have shown that the morphology of the Cu component is critically dependent on reduction conditions. XAFS amplitude reductions have been identified which originate in small particle sizes and changes in the suboxidation state of the catalyst. Cluster XANES calculations have shown (i) that the loss of long-range pair correlations results in near-edge structure changes compatible with the experimentally observed XANES data and (ii) that the XANES structure observed for the catalyst requires an fcc coordination with at least five to six shells.

The detailed mechanism underlying the observed XAFS changes is at the time of writing unknown. Possible explanations include the reversible formation of a highly dispersed oxide phase, the dissolution of oxygen in the Cu lattice, or particle morphology changes similar to the wetting/nonwetting transitions observed by Clausen *et al.* [37]. Future work will address the possibility of particle morphology changes by *in situ* XRD and XAFS studies. Further XAFS studies of the interaction between Cu and oxygen are currently being carried out by the author using a new *in situ* TEY setup.

In situ XAFS studies of the catalyst have also shown that CO₂ does not dissociate on the surface of the Cu particles under methanol synthesis conditions. An earlier result which indicated the opposite could not be reproduced.

Finally, the first TEY experiment at elevated pressure ($p = 40$ atm) has been carried out while exposing the catalyst to synthesis gas. The results confirm earlier conclusions that the active state of the Cu component in the catalyst is at least predominantly metallic.

5.5. References

- [1] D.L. Trimm, M.S. Wainwright, *Catalysis Today* 6 (1990) 261.
- [2] G.W. Bridger, M.S. Spencer, *Methanol Synthesis*, in: *Catalyst Handbook*, ed. by M.V. Twigg (Wolfe Publishing Ltd. London, 1989) 441.
- [3] *The Economist* March 11 (1995) 131.
- [4] G.C. Chinchin, K. Mansfield, M.S. Spencer, *Chemtech* 20 (1990) 692.
- [5] J.R. Rostrup-Nielsen, *Catalysis Today* 21 (1994) 257.
- [6] K.C. Waugh, *Catalysis Today* 15 (1992) 51.

- [7] J.W.M.H. Geerts, J.H.B.J. Hoebink, K. van der Wiele, *Catalysis Today* 6 (1990) 613.
- [8] J.C.J. Bart, R.P.A. Sneeden, *Catalysis Today* 2 (1987) 1.
- [9] G. Ghiotti, F. Boccuzzi, *Catal. Rev. - Sci. Eng.* 29 (1987) 151.
- [10] J.P. Hindermann, G.J. Hutchings, A. Kiennemann, *Catal. Rev. - Sci. Eng.* 35 (1993) 1.
- [11] K.C. Waugh, *Catalysis Today* 18 (1993) 147.
- [12] G.C. Chinchin, P.J. Denny, J.R. Jennings, M.S. Spencer, K.C. Waugh, *Appl. Catal.* 36 (1988) 1.
- [13] A.Y. Rozovskii, *Russian Chem. Rev.* 58 (1989) 41.
- [14] H. Goehna, P. Koenig, *Chemtech* 24 (1994) 36.
- [15] M. Muhler, E. Törnqvist, L.P. Nielsen, B.S. Clausen, H. Topsoe, *Catal. Lett.* 25 (1994) 1.
- [16] H. Berndt, V. Briehn, S. Evert, D. Gutschick, W. Kotowski, *Catal. Lett.* 14 (1992) 185.
- [17] K. Kern, *Vacuum* 41 (1990) 389.
- [18] R. Burch, S.E. Golunski, M.S. Spencer, *Catal. Lett.* 6 (1990) 152.
- [19] J.C. Frost, *Nature* 334 (1988) 577.
- [20] R. Burch, S.E. Golunski, M.S. Spencer, *J. Chem. Soc. Faraday Trans.* 86 (1990) 2683.
- [21] L.E.Y. Nonneman, V. Ponec, *Catal. Lett.* 7 (1990) 213.
- [22] Y. Kanai, T. Watanabe, T. Fujitani, M. Saito, J. Nakamura, T. Uchijima, *Catal. Lett.* 27 (1994) 67.
- [23] K.C. Waugh, *Catal. Lett.* 7 (1991) 345.
- [24] E.A. Shaw, T. Rayment, A.P. Walker, J.R. Jennings, R.M. Lambert, *J. Catal.* 126 (1990) 219.
- [25] E.A. Shaw, A.P. Walker, T. Rayment, R.M. Lambert, *J. Catal.* 134 (1992) 747.
- [26] M.S. Spencer, *Catalysis Today* 12 (1992) 453.
- [27] M.S. Spencer, R. Burch, S.E. Golunski, *J. Catal.* 126 (1990) 311.
- [28] M.S. Spencer, R. Burch, S.E. Golunski, *J. Chem. Soc. Faraday Trans.* 86 (1990) 3151.
- [29] G.C. Chinchin, M.S. Spencer, K.C. Waugh, D.A. Whan, *Appl. Catal.* 32 (1987) 371.
- [30] C.T. Campbell, *Appl. Catal.* 32 (1987) 367.
- [31] M. Muhler, L.P. Nielsen, E. Törnqvist, B.S. Clausen, H. Topsoe, *Catal. Lett.* 14 (1992) 241.

- [32] C.V. Ovesen, B.S. Clausen, B.S. Hammershoi, G. Steffensen, T. Askgaard, I. Chorkendorff, J.K. Norskov, P.B. Rasmussen, P. Stoltze, P. Taylor, *J. Catal.* 158 (1996) 170.
- [33] T.S. Askgaard, J.K. Norskov, C.V. Ovesen, P. Stoltze, *J. Catal.* 156 (1995) 229.
- [34] S. Bailey, G.F. Froment, J.W. Snoeck, K.C. Waugh, *Catal. Lett.* 30 (1995) 99.
- [35] R.A. Hadden, P.J. Lambert, C. Ranson, *Appl. Catal. A:General* 122 (1995) L1.
- [36] J. Yoshihara, S.C. Parker, A. Schafer, C.T. Campbell, *Catal. Lett.* 31 (1995) 313.
- [37] B.S. Clausen, L. Gråbak, C.V. Ovesen, J. Schiøtz, K.W. Jacobsen, J.K. Norskov, *Topics Catal.* 1 (1994) 367.
- [38] M. Bowker, R.A. Hadden, H. Houghton, J.N.K. Hyland, K.C. Waugh, *J. Catal.* 109 (1988) 263.
- [39] Y.B. Kagan, L.G. Liberov, E.V. Slivinskii, S.M. Loktev, S.M. Lin, A.Y. Rozovskii, A.N. Bashkirov, *Dokl. Akad. Nauk. SSSR* 221 (1975) 1093.
- [40] G.C. Chinchin, P.J. Denny, D.G. Parker, M.S. Spencer, D.A. Whan, *Appl. Catal.* 30 (1987) 333.
- [41] G. Liu, D. Willcox, M. Garland, H.H. Kung, *J. Catal.* 96 (1985) 251.
- [42] S.D. Jackson, *J. Catal.* 108 (1987) 250.
- [43] G.C. Chinchin, K.C. Waugh, D.A. Whan, *Appl. Catal.* 25 (1986) 101.
- [44] K.M. Vanden Bussche, G.F. Froment, *Appl. Catal. A:General* 112 (1994) 37.
- [45] G.D. Sizgek, H.E. Curry-Hide, M.S. Wainwright, *Appl. Catal. A:General* 115 (1994) 15.
- [46] P.B. Himelfarb, G.W. Simmons, K. Klier, R.G. Herman, *J. Catal.* 93 (1985) 442.
- [47] S.G. Neophytides, A.J. Marchi, G.F. Froment, *Appl. Catal. A:General* 86 (1992) 45.
- [48] J. Szanyi, D.W. Goodman, *Catal. Lett.* 10 (1991) 383.
- [49] P.B. Rasmussen, M. Kazuta, I. Chorkendorff, *Surf. Sci.* 318 (1994) 267.
- [50] P.B. Rasmussen, P.M. Holmblad, T. Askgaard, C.V. Ovesen, P. Stoltze, J.K. Norskov, I. Chorkendorff, *Catal. Lett.* 26 (1994) 373.
- [51] P.A. Taylor, P.B. Rasmussen, C.V. Ovesen, P. Stoltze, I. Chorkendorff, *Surf. Sci.* 261 (1992) 191.
- [52] D.S. King, D.A. Mantell, R.R. Cavanagh, *J. Chem. Phys.* 82 (1985) 1046.
- [53] G.C. Chinchin, M.S. Spencer, K.C. Waugh, D.A. Whan, *J. Chem. Soc. Faraday Trans. I* 83 (1987) 2193.
- [54] B. Denise, R.P.A. Sneed, B. Beguin, O. Cherifi, *Appl. Catal.* 30 (1987) 353.
- [55] G.C. Chinchin, K.C. Waugh, *J. Catal.* 97 (1986) 280.
- [56] H. Berndt, V. Briehn, S. Evert, *Appl. Catal. A:General* 86 (1992) 65.

- [57] M. Muhler, L.P. Nielsen, E. Törnqvist, B.S. Clausen, H. Topsoe, *Catal. Lett.* 17 (1993) 375.
- [58] H. Berndt, V. Briehn, S. Evert, *J. Mol. Catal.* 73 (1992) 203.
- [59] G. Wrobel, L. Jalowiecki, J.P. Bonnelle, F. Bali, A. Bettahar, *New J. Chem.* 11 (1987) 715.
- [60] J. Nakamura, J.A. Rodriguez, C.T. Campbell, *J. Phys: Condens. Matter* 1 (1989) SB149.
- [61] G.D. Moggridge, T. Rayment, R.M. Ormerod, M.A. Morris, R.M. Lambert, *Nature* 358 (1992) 658.
- [62] B.S. Clausen, G. Steffensen, B. Fabius, J. Villadsen, R. Feidenhans'l, H. Topsoe, *J. Catal.* 132 (1991) 524.
- [63] B.S. Clausen, H. Topsoe, *Catalysis Today* 9 (1991) 189.
- [64] J.W. Couves, J.M. Thomas, D. Waller, R.H. Jones, A.J. Dent, G.E. Derbyshire, G.N. Greaves, *Nature* 354 (1991) 465.
- [65] L.S. Kau, K.O. Hodgson, E.I. Solomon, *J. Am. Chem. Soc.* 111 (1989) 7103.
- [66] T.L. Neils, J.M. Burlitch, *J. Catal.* 118 (1989) 79.
- [67] B.S. Clausen, B. Lengeler, B.S. Rasmussen, W. Niemann, H. Topsoe, *J. Phys. (Paris)* 47 C8 (1986) 237.
- [68] K. Tohji, Y. Udagawa, T. Mizushima, A. Ueno, *J. Phys. Chem.* 89 (1985) 5671.
- [69] I. Chorkendorff, P.B. Rasmussen, H. Christoffersen, P.A. Taylor, *Surf. Sci.* 287 (1993) 208.
- [70] P.B. Rasmussen, P.A. Taylor, I. Chorkendorff, *Surf. Sci.* 270 (1992) 352.
- [71] J. Als-Nielsen, G. Grübel, B.S. Clausen, *Nucl. Instrum. Methods B* 97 (1995) 522.
- [72] B.S. Clausen, L. Gråbak, H. Topsoe, L.B. Hansen, P. Stoltze, J.K. Norskov, O.H. Nielsen, *J. Catal.* 141 (1993) 368.
- [73] B.S. Clausen, H. Topsoe, L.B. Hansen, P. Stoltze, J.K. Norskov, *Catalysis Today* 21 (1994) 49.
- [74] B.S. Clausen, L. Gråbak, G. Steffensen, P.L. Hansen, H. Topsoe, *Catal. Lett.* 20 (1993) 23.
- [75] G.C. Chinchin, C.M. Hay, H.D. Vandervell, K.C. Waugh, *J. Catal.* 103 (1987) 79.
- [76] G.D. Moggridge, S.L.M. Schroeder, R.M. Lambert, T. Rayment, *Nucl. Instrum. Methods B* 97 (1995) 28.
- [77] P. Scherrer, *Göttinger Nachrichten* 2 (1918) 98.
- [78] H.P. Klug, L.E. Alexander, *X-ray Diffraction Procedures* (John Wiley & Sons, New York, 1974).
- [79] J.I. Langford, D. Louer, *Rep. Prog. Phys.* 59 (1996) 131.

- [80] B.E. Warren, B.L. Auerbach, J. Appl. Phys. 21 (1950) 595.
- [81] G. Vlaic, J.C.J. Bart, W. Cavigiolo, S. Mobilio, Chem. Phys. Lett. 76 (1980) 453.
- [82] G. Vlaic, J.C.J. Bart, W. Cavigiolo, B. Pianzola, S. Mobilio, J. Catal. 96 (1985) 314.
- [83] B.S. Clausen, B. Lengeler, B.S. Rasmussen, J. Phys. Chem. 89 (1985) 2319.
- [84] L.S. Kau, E.I. Solomon, K.O. Hodgson, J. Phys. (Paris) 47 C8 (1986) 289.
- [85] G. Sankar, S. Vasudevan, C.N.R. Rao, J. Chem. Phys. 85 (1986) 2291.
- [86] J.E. Hahn, R.A. Scott, A. Hodgson, S. Doniach, S.R. Desjardins, E.I. Solomon, Chem. Phys. Lett. 88 (1982) 595.
- [87] L.S. Kau, D.J. Spira-Solomon, J.E. Penner-Hahn, A. Hodgson, E.I. Solomon, J. Am. Chem. Soc. 109 (1987) 6433.
- [88] K. Klier, Adv. Catal. 31 (1982) 243.
- [89] P.B. Himelfarb, G.W. Simmons, K. Klier, M. Joseyacaman, ACS Symp. Ser. 288 (1985) 351.
- [90] J.M. Dominquez, G.W. Simmons, K. Klier, J. Mol. Catal. 20 (1983) 369.
- [91] L.B. Hansen, P. Stoltze, J.K. Norskov, B.S. Clausen, W. Niemann, Phys. Rev. Lett. 64 (1990) 3155.
- [92] R.W. Joyner, K.J. Martin, P. Meehan, J. Phys. C 20 (1987) 4005.
- [93] M. Vaarkamp, *The Structure and Catalytic Properties of Supported Platinum Catalysts* (Technical University, Eindhoven, 1992).
- [94] A.F. Wells, *Structural Inorganic Chemistry* (Clarendon Press, Oxford, 1984).
- [95] R.G. Herman, K. Klier, G.W. Simmons, B.P. Finn, J.B. Bulko, T.P. Kobylinski, J. Catal. 56 (1979) 407.
- [96] R.A. Scott, J.E. Hahn, S. Doniach, H. Freeman, K.O. Hodgson, J. Am. Chem. Soc. 104 (1982) 5364.
- [97] R.B. Gregor, F.W. Lytle, J. Catal. 63 (1980) 476.
- [98] C. Rehren, G. Isaac, R. Schlögl, G. Ertl, Catal. Lett. 11 (1991) 253.
- [99] B. Pettinger, X.H. Bao, I. Wilcock, M. Muhler, R. Schlögl, G. Ertl, Angew. Chemie - Int. Ed. 33 (1994) 85.
- [100] H. Schubert, U. Tegtmeier, R. Schlögl, Catal. Lett. 28 (1994) 383.
- [101] X. Bao, M. Muhler, B. Pettinger, R. Schlögl, G. Ertl, Catal. Lett. 22 (1993) 215.
- [102] T.N. Rhodin, J. Am. Chem. Soc. 73 (1951) 3143.
- [103] T.N. Rhodin, J. Am. Chem. Soc. 72 (1950) 5102.
- [104] D.T. Ling, J.N. Miller, P. Pianetta, D.L. Weissman, I. Lindau, W.E. Spicer, J. Vac. Sci. Technol. 15 (1978) 495.

- [105] F.H.P.M. Habraken, C.M.A.M. Mesters, G.A. Bootsma, Surf. Sci. 97 (1980) 264.
- [106] M.J. Braithwaite, R.W. Joyner, M.W. Roberts, Faraday Discuss. Chem. Soc. 60 (1975) 89.
- [107] G. Wulff, Z. Kristall. 34 (1901) 449.
- [108] S. Gota, M. Gautier, L. Douillard, N. Thomat, J.P. Duraud, P. Le Fevre, Surf. Sci. 323 (1995) 163.
- [109] S.I. Zabinsky, J.J. Rehr, A. Ankudinov, R.C. Albers, M.J. Eller, Phys. Rev. B 52 (1995) 2995.
- [110] E. Sevillano, H. Meuth, J.J. Rehr, Phys. Rev. B 20 (1979) 4908.
- [111] E.D. Crozier, J.J. Rehr, R. Ingalls, *Amorphous and Liquid Systems*, in: X-ray Absorption: Principles, Applications, Techniques of EXAFS, SEXAFS and XANES, ed. by D.C. Koningsberger and R. Prins (Wiley-Interscience, New York, 1988) 373.
- [112] J. Mustre de Leon, J.J. Rehr, S.I. Zabinsky, R.C. Albers, Phys. Rev. B 44 (1991) 4146.
- [113] C. Kittel, *Introduction to Solid State Physics* (Wiley, New York, 1986).
- [114] G. Sankar, J.M. Thomas, D. Waller, J.W. Couves, C.R.A. Catlow, G.N. Greaves, J. Phys. Chem. 96 (1992) 7485.
- [115] R. Frahm, J. Barbee, T.W., W. Warburton, Phys. Rev. B 44 (1991) 2822.